

Soft-gluon corrections in top-quark production

Nikolaos Kidonakis

*Department of Physics, Kennesaw State University,
Kennesaw, GA 30144, USA*

Abstract

I review calculations of soft-gluon corrections for top-quark production in hadron collisions. I describe theoretical formalisms for their resummation and for finite-order expansions. I show that soft-gluon corrections are dominant for a large number of top-quark processes. I discuss top-antitop pair production as well as single-top production, including total cross sections and differential distributions, and compare with data from the LHC and the Tevatron. I also discuss top-quark production in association with charged Higgs bosons, Z bosons, and other particles in models of new physics.

1 Introduction

Top-quark physics is a central element in the exploration of particle physics at hadron colliders. The top quark occupies a special place as the heaviest elementary particle to have been found, and the only quark that decays before it can hadronize. It was discovered via the top-antitop pair production process in proton-antiproton collisions at the Fermilab Tevatron by the CDF and D0 Collaborations in 1995 [1, 2]. Single-top production events were also first seen at the Tevatron [3, 4]. The top quark was later rediscovered at the LHC in $t\bar{t}$ [5, 6] processes. The LHC now serves as a top-quark factory.

In this paper I review top-quark production in hadron colliders, focusing on higher-order corrections from soft-gluon resummation. There is a very long history of resummations for top-pair production, Refs. [7-67], for single-top production, Refs. [68-77], as well as for top-quark production in models of new physics, Refs. [78-84].

Next-to-leading order (NLO) [85–87] and next-to-next-to-leading order (NNLO) [88–91] corrections have been available for top-pair production for some time. For single-top production, NLO corrections for the t and s channels [92] and for tW production [93] are also known, while NNLO corrections [94–96] have been calculated for the t -channel. Higher-order soft-gluon corrections can further improve the NLO and NNLO results.

In Section 2, I begin with a brief history of soft-gluon resummation, followed by a general discussion of higher-order soft-gluon corrections, factorization, renormalization-group evolution, resummation, and expansions at NLO, NNLO, and next-to-next-to-next-to-leading order (N^3 LO).

In Section 3, I continue with a review of the cusp anomalous dimension and of soft anomalous dimension matrices for $t\bar{t}$ production through two loops. In Section 4, I provide results for the total $t\bar{t}$ cross sections, the top-quark transverse momentum, p_T , distributions, and the top-quark rapidity distributions at the LHC and the Tevatron, as well as the forward-backward asymmetry at the Tevatron.

In Section 5, I discuss single-top production, including t -channel and s -channel production, and tW production, and I present total cross sections and top-quark p_T and rapidity distributions. In Section 6, I discuss top-quark production in association with a charged Higgs boson, and in association with gauge bosons via anomalous couplings in new-physics models. I conclude with a summary in Section 7.

2 Soft-gluon corrections

Soft-gluon corrections arise from the emission of low-energy gluons, and they result from incomplete cancellations of infrared divergences between virtual diagrams and diagrams with real emission.

These corrections appear in the perturbative series as plus distributions involving logarithms of a variable that measures the kinematical distance from threshold. For the n th-order perturbative corrections, the leading logarithms are those with the highest power, $2n - 1$; the next-to-leading logarithms have a power of $2n - 2$; etc. The effects of soft-gluon corrections are particularly relevant near partonic threshold. At partonic threshold there is no energy for additional radiation, but the top quark may have non-zero momentum and is not restricted to be produced at rest. Thus, partonic threshold is a more general concept than production or absolute threshold, where the top quark is produced at rest.

For top-antitop production, several threshold variables have been used for resummation. In single-particle-inclusive (1PI) kinematics, the partonic threshold variable is $s_4 = s + t + u - \sum m^2$ where s , t , and u are the standard kinematical variables and the sum is over the masses squared of all particles in the scattering. At partonic threshold, $s_4 \rightarrow 0$. In pair-invariant-mass (PIM) kinematics, the partonic threshold variable is $1 - z = 1 - M_{t\bar{t}}^2/s$, where $M_{t\bar{t}}$ is the invariant mass of the top-antitop pair; at partonic threshold $z \rightarrow 1$. In resummation using absolute threshold - a special limiting case of partonic threshold as we discussed above - the threshold variable is $\beta = \sqrt{1 - 4m_t^2/s}$, where m_t is the top-quark mass; at absolute threshold, $\beta \rightarrow 0$.

Formalisms that use partonic threshold in 1PI or PIM kinematics involve a general resummation for double-differential distributions, from which single distributions or total cross sections can be derived by appropriate integrations. Formalisms that use absolute threshold are limited only to total cross sections.

Similarly, 1PI kinematics have been used in resummations for single-top production using the threshold variable s_4 .

Soft-gluon corrections are dominant near threshold and usually even far from threshold. These corrections can be formally resummed to all orders in perturbative QCD. This resummation, i.e. exponentiation, follows from the factorization properties of the cross section and from the renormalization-group evolution of the functions in the factorized form.

Leading-logarithm (LL) resummations and their finite-order expansions for top-antitop pair production were developed and used in various formalisms in Refs. [7–12, 15, 18]. Next-to-leading-logarithm (NLL) resummations and their expansions were developed and used for double-differential cross sections in Refs. [13, 17, 20–25] using partonic threshold, and in Refs. [19, 26] for only total cross sections. Corrections beyond NLL in expansions were calculated in Refs. [23, 25, 27, 28, 30, 31, 33]. Next-to-next-to-leading-logarithm (NNLL) resummations and

expansions were developed in Refs. [35–41, 45, 48–51].

Leading logarithms can be resummed in terms of universal terms for the emission of collinear and soft gluons; these universal terms only depend on the identity of the incoming and outgoing partons. However, at NLL accuracy and beyond [13, 17] resummation involves the process-dependent color exchange in the hard-scattering process.

More explicitly, in 1PI kinematics the soft-gluon terms are of the form $[\ln^k(s_4/m_t^2)/s_4]_+$ where $k \leq 2n - 1$ for the n th-order perturbative corrections, and s_4 is the kinematical distance from partonic threshold described above. We define

$$\mathcal{D}_k(s_4) \equiv \left[\frac{\ln^k(s_4/m_t^2)}{s_4} \right]_+ = \frac{\ln^k(s_4/m_t^2)}{s_4} \theta(s_4 - \Delta) + \frac{1}{k+1} \ln^{k+1} \left(\frac{\Delta}{m_t^2} \right) \delta(s_4), \quad (1)$$

where Δ is a small parameter that separates the hard-gluon, $s_4 > \Delta$, and soft-gluon, $s_4 < \Delta$, regions.

In PIM kinematics the soft-gluon terms are of the form $[\ln^k(1-z)/(1-z)]_+$, where again $k \leq 2n - 1$ for the n th-order perturbative corrections, and $1-z$ is the kinematical distance from partonic threshold described above. We define

$$\mathcal{D}_k(z) \equiv \left[\frac{\ln^k(1-z)}{1-z} \right]_+ = \frac{\ln^k(1-z)}{1-z} \theta(1-z - \Delta) + \frac{1}{k+1} \ln^{k+1}(\Delta) \delta(1-z), \quad (2)$$

where, again, Δ is a small parameter that separates the hard-gluon, $1-z > \Delta$, and soft-gluon, $1-z < \Delta$, regions.

2.1 Factorization and Resummation

We consider top-quark production in proton-proton collisions at the LHC,

$$p(p_A) + p(p_B) \rightarrow t(p_t) + X \quad (3)$$

and proton-antiproton collisions at the Tevatron

$$p(p_A) + \bar{p}(p_B) \rightarrow t(p_t) + X \quad (4)$$

where t denotes the observed top quark, with X all additional final-state particles. The partonic processes involved are of the form

$$f_1(p_1) + f_2(p_2) \rightarrow t(p_t) + X \quad (5)$$

where f_1 and f_2 are partons (quarks and/or gluons). We define the usual kinematical variables $s = (p_1 + p_2)^2$, $t = (p_1 - p_t)^2$, $u = (p_2 - p_t)^2$. We also define, as before, the 1PI partonic threshold variable $s_4 = s + t + u - \sum m^2$.

The factorized form of the (differential) cross section may be written in 1PI kinematics as

$$d\sigma^{pp \rightarrow tX} = \sum_{f_1, f_2} \int dx_1 dx_2 \phi_{f_1/h_1}(x_1, \mu_F) \phi_{f_2/h_2}(x_2, \mu_F) \hat{\sigma}^{f_1 f_2 \rightarrow tX}(s_4, s, t, u, \mu_F, \mu_R) \quad (6)$$

where μ_F is the factorization scale and μ_R is the renormalization scale. A similar expression applies to PIM kinematics. The parton distribution functions (pdf), ϕ , describe the fraction of the proton momentum carried by the partons, with x_1 and x_2 the momentum fractions of partons f_1 and f_2 in protons A and B respectively.

Soft-gluon corrections in the partonic cross section, $\hat{\sigma}_{f_1 f_2 \rightarrow tX}$, contribute terms with plus distributions of logarithms of s_4 or $1 - z$, defined via their integral with the pdf. In 1PI kinematics

$$\int_0^{s_4^{\max}} ds_4 \phi(s_4) \left[\frac{\ln^k(s_4/m_t^2)}{s_4} \right]_+ \equiv \int_0^{s_4^{\max}} ds_4 \frac{\ln^k(s_4/m_t^2)}{s_4} [\phi(s_4) - \phi(0)] + \frac{1}{k+1} \ln^{k+1} \left(\frac{s_4^{\max}}{m_t^2} \right) \phi(0), \quad (7)$$

while in PIM kinematics

$$\int_{z_{\min}}^1 dz \phi(z) \left[\frac{\ln^k(1-z)}{1-z} \right]_+ \equiv \int_{z_{\min}}^1 dz \frac{\ln^k(1-z)}{1-z} [\phi(z) - \phi(1)] + \frac{1}{k+1} \ln^{k+1}(1-z_{\min}) \phi(1). \quad (8)$$

These are equivalent definitions to Eqs. (1) and (2), respectively.

The resummation of soft-gluon contributions results from the factorization properties of the cross section in moment space. Moments of the partonic cross section are defined by $\hat{\sigma}(N) = \int (ds_4/s) e^{-Ns_4/s} \hat{\sigma}(s_4)$ in 1PI kinematics, and $\hat{\sigma}(N) = \int dz z^{N-1} \hat{\sigma}(z)$ in PIM kinematics. Logarithms of s_4 or $1 - z$ transform in moment space into logarithms of N , which exponentiate.

We write the moment-space partonic cross section, in $4 - \epsilon$ dimensions, in factorized form, as

$$\sigma^{f_1 f_2 \rightarrow tX}(N, \epsilon) = \phi_{f_1/f_1}(N, \mu_F, \epsilon) \phi_{f_2/f_2}(N, \mu_F, \epsilon) \hat{\sigma}^{f_1 f_2 \rightarrow tX}(N, \mu_F, \mu_R) \quad (9)$$

with $\phi(N) = \int_0^1 dx x^{N-1} \phi(x)$.

We then refactorize the cross section [13, 17] as

$$\begin{aligned} \sigma^{f_1 f_2 \rightarrow tX}(N, \epsilon) &= H_{IL}^{f_1 f_2 \rightarrow tX}(\alpha_s(\mu_R)) S_{LI}^{f_1 f_2 \rightarrow tX} \left(\frac{m_t}{N \mu_F}, \alpha_s(\mu_R) \right) \\ &\times \prod J_{\text{in}}(N, \mu_F, \epsilon) \prod J_{\text{out}}(N, \mu_F, \epsilon), \end{aligned} \quad (10)$$

where I and L are color indices.

The $H_{IL}^{f_1 f_2 \rightarrow tX}$ is the hard-scattering function that does not depend on N , and it describes contributions from the amplitude and the complex conjugate of the amplitude for the process. The soft-gluon function $S_{LI}^{f_1 f_2 \rightarrow tX}$ describes the coupling of soft gluons to the partons in the scattering. The analytical form of H_{IL} and S_{LI} depends on the process, and in general both functions are matrices in color space in the partonic scattering. The J_{in} and J_{out} are jet functions that describe universal soft and collinear emission from incoming and outgoing massless partons.

The N -dependence of the soft matrix S_{LI} can be resummed via renormalization group evolution [13, 17]. We have

$$S_{LI}^b = (Z_S^\dagger)_{LC} S_{CD} Z_{S, DI} \quad (11)$$

where S^b is the unrenormalized quantity and Z_S is a matrix of renormalization constants. Thus S_{LI} satisfies the renormalization group equation

$$\left(\mu \frac{\partial}{\partial \mu} + \beta(g_s) \frac{\partial}{\partial g_s} \right) S_{LI} = -(\Gamma_S^\dagger)_{LK} S_{KI} - S_{LK} (\Gamma_S)_{KI} \quad (12)$$

where $g_s^2 = 4\pi\alpha_s$, and β is the QCD beta function

$$\beta(\alpha_s) \equiv \frac{1}{2} \frac{d \ln \alpha_s}{d \ln \mu} = - \sum_{n=0}^{\infty} \beta_n \left(\frac{\alpha_s}{4\pi} \right)^{n+1} \quad (13)$$

where $\beta_0 = (11C_A - 2n_f)/3$, $C_A = N_c$, with $N_c = 3$ the number of colors, and n_f is the number of light quark flavors ($n_f = 5$ for top production).

The soft anomalous dimension, Γ_S , controls the evolution of the soft function S . We determine Γ_S from the coefficients of the ultraviolet poles of eikonal diagrams. In dimensional regularization Z_S has $1/\epsilon$ poles, and Γ_S is given in terms of the residue of Z_S [13,17]. In general, Γ_S is a matrix in color space as well as a function of the kinematic variables s, t, u .

The resummed cross section in moment space is derived from the renormalization-group evolution of the functions in the factorized cross section, and can be written as

$$\begin{aligned} \hat{\sigma}_{\text{resum}}^{f_1 f_2 \rightarrow tX}(N) &= \exp \left[\sum_{i=1,2} E_i(N_i) \right] \exp \left[\sum_j E'_j(N'_j) \right] \\ &\times \exp \left[\sum_{i=1,2} 2 \int_{\mu_F}^{\sqrt{s}} \frac{d\mu}{\mu} \gamma_{i/i}(\tilde{N}_i, \alpha_s(\mu)) \right] \\ &\times \text{tr} \left\{ H^{f_1 f_2 \rightarrow tX}(\alpha_s(\sqrt{s})) \exp \left[\int_{\sqrt{s}}^{\sqrt{s}/\tilde{N}'} \frac{d\mu}{\mu} \Gamma_S^\dagger{}^{f_1 f_2 \rightarrow tX}(\alpha_s(\mu)) \right] \right. \\ &\left. \times S^{f_1 f_2 \rightarrow tX} \left(\alpha_s \left(\frac{\sqrt{s}}{\tilde{N}'} \right) \right) \exp \left[\int_{\sqrt{s}}^{\sqrt{s}/\tilde{N}'} \frac{d\mu}{\mu} \Gamma_S^{f_1 f_2 \rightarrow tX}(\alpha_s(\mu)) \right] \right\} \end{aligned} \quad (14)$$

where the trace is taken of the product of the color-space hard and soft matrices, and the exponents of Γ_S .

The collinear-gluon and soft-gluon contributions from the initial-state partons are resummed in the first exponential in Eq. (14), with exponent

$$E_i(N_i) = \int_0^1 dz \frac{z^{N_i-1} - 1}{1-z} \left\{ \int_1^{(1-z)^2} \frac{d\lambda}{\lambda} A_i(\alpha_s(\lambda s)) + D_i[\alpha_s((1-z)^2 s)] \right\}. \quad (15)$$

Here we have defined $N_1 = N(m_t^2 - u)/m_t^2$ and $N_2 = N(m_t^2 - t)/m_t^2$. The perturbative series for A_i is written as $A_i = \sum_{n=1}^{\infty} (\alpha_s/\pi)^n A_i^{(n)}$, with $A_i^{(1)} = C_i$ [97] where $C_i = C_F = (N_c^2 - 1)/(2N_c)$ for a quark or antiquark, while $C_i = C_A$ for a gluon; and $A_i^{(2)} = C_i K/2$ [98] where $K = C_A (67/18 - \zeta_2) - 5n_f/9$ [99], with $\zeta_2 = \pi^2/6$. Also the perturbative series for D_i is written as $D_i = \sum_{n=1}^{\infty} (\alpha_s/\pi)^n D_i^{(n)}$, with $D_i^{(1)} = 0$ in Feynman gauge.

The collinear-gluon and soft-gluon contributions from final-state massless quarks and/or gluons are resummed in the second exponential, with exponent

$$E'_j(N') = \int_0^1 dz \frac{z^{N'-1} - 1}{1-z} \left\{ \int_{(1-z)^2}^{1-z} \frac{d\lambda}{\lambda} A_j(\alpha_s(\lambda s)) + B_j[\alpha_s((1-z)s)] \right. \\ \left. + D_j[\alpha_s((1-z)^2 s)] \right\} \quad (16)$$

where we have defined $N' = Ns/m_t^2$. The perturbative series for B_j is written as $B_j = \sum_{n=1}^{\infty} (\alpha_s/\pi)^n B_j^{(n)}$, with $B_q^{(1)} = -3C_F/4$ for a quark or antiquark, and $B_g^{(1)} = -\beta_0/4$ for a gluon [97, 98]. Note that this exponent is not needed in $t\bar{t}$ or tW production but it is used in s -channel and t -channel single-top production.

The factorization-scale dependence in the third exponential is given in moment space by the anomalous dimension of $\phi_{i/i}$, which is $\gamma_{i/i} = -A_i \ln \tilde{N}_i + \gamma_i$, where $\tilde{N}_i = N_i e^{\gamma_E}$ with γ_E the Euler constant, and $\gamma_i = \sum_{n=1}^{\infty} (\alpha_s/\pi)^n \gamma_i^{(n)}$ with $\gamma_q^{(1)} = 3C_F/4$, $\gamma_g^{(1)} = \beta_0/4$.

The perturbative series for the hard function H and the soft function S are written as $H = \alpha_s^{d_{\alpha_s}} \sum_{n=0}^{\infty} (\alpha_s/\pi)^n H^{(n)}$ and $S = \sum_{n=0}^{\infty} (\alpha_s/\pi)^n S^{(n)}$, respectively, where d_{α_s} denotes the power of α_s in the leading-order (LO) cross section. The LO cross section for each partonic process is given by the trace of the product of the lowest-order hard and soft matrices: $\sigma^B = \alpha_s^{d_{\alpha_s}} \text{tr}[H^{(0)} S^{(0)}]$.

Noncollinear soft-gluon emission is described by the soft anomalous dimension Γ_S , with perturbative expansion

$$\Gamma_S = \sum_{n=1}^{\infty} \left(\frac{\alpha_s}{\pi} \right)^n \Gamma_S^{(n)} \quad (17)$$

The first term in the series, $\Gamma_S^{(1)}$, requires one-loop calculations and is needed for NLL resummation, while $\Gamma_S^{(2)}$ requires two-loop calculations and is needed for NNLL resummation.

2.2 Methods and prescriptions

There are numerous and very substantive differences between the various resummation approaches in the literature, which have been detailed previously in Refs. [53, 60]. Some formalisms have been developed to do the resummation only for the total cross section while others are for the double-differential cross section; some formalisms use moment-space perturbative QCD while others use Soft-Collinear Effective Theory (SCET). The treatment of sub-leading logarithms in different formalisms and the approach to deal with infrared divergences via prescriptions or finite-order expansions lead to large differences in numerical results.

The more general double-differential approach to resummation can be expressed in 1PI kinematics for the differential cross section in top-quark transverse momentum and rapidity, $d\sigma/dp_T dy$, where the soft limit is $s_4 \rightarrow 0$, or in PIM kinematics for the differential cross section in top-pair invariant mass and scattering angle, $d\sigma/dM_{t\bar{t}} d\cos\theta$, where the soft limit is $z \rightarrow 1$. Such double-differential approaches have been developed in moment-space in QCD, Refs. [13, 17, 20, 22–25, 27, 28, 30, 49, 60, 61, 64], as well as in SCET, Refs. [40, 41, 45, 50]. Double-differential distributions, single-differential distributions, and total cross sections can all be derived via the above formalisms. Resummations that are developed for the total cross section

only refer to production (or absolute) threshold and resum logarithms of $\beta = \sqrt{1 - 4m_t^2/s}$, Refs. [19, 31, 38, 47, 48, 55]. The soft limit here is the production threshold limit $\beta \rightarrow 0$ (where the top quark velocities are zero), which is a special case of the more general partonic threshold.

The resummed cross section encounters infrared divergences that require a prescription to be dealt with, and the choice of prescription is to an extent arbitrary. Moreover, the numerical results depend greatly on the prescription, and differences between prescriptions are typically larger than corrections beyond NNLO. In order to avoid arbitrary prescription dependence, an excellent approach is to expand the resummed cross section to a fixed order, usually NNLO or N³LO; this gives better control of subleading terms.

The relative size of soft-gluon corrections has been argued about since the 1990's. The LL results in Refs. [7–9] and [10, 12, 18] argued for large effects. The LL results in [11, 15], using the minimal prescription, argued for tiny corrections, one or two orders of magnitude smaller. Similarly at NLL, the results in Ref. [19], which were based on the minimal prescription, were much smaller than the results in Refs. [23, 24], which were based on Refs. [13, 17, 20] and used fixed-order expansions. In Ref. [55] the predictions with minimal prescription are small for both Tevatron and LHC energies and they account for only a very small fraction of the NNLO corrections. In contrast the predictions in Ref. [27, 33] and the NNLL predictions in Refs. [49, 51], using fixed-order expansions, predicted the NNLO corrections, which are large, extremely well.

2.3 NLO, NNLO, and N³LO expansions

Here we present expansions of the resummed cross section through N³LO. We use the D_k notation for the logarithmic plus distributions of Eqs. (1) and (2). We give results for 1PI kinematics first.

The NLO soft-gluon corrections from the expansion of the resummed cross section are given by

$$\hat{\sigma}^{(1)} = \sigma^B \frac{\alpha_s(\mu_R)}{\pi} \{c_3 \mathcal{D}_1(s_4) + c_2 \mathcal{D}_0(s_4)\} + \frac{\alpha_s^{d_{\alpha_s}+1}(\mu_R)}{\pi} A^c \mathcal{D}_0(s_4) \quad (18)$$

where σ^B is the LO term. The LL coefficient is

$$c_3 = \sum_i 2 A_i^{(1)} - \sum_j A_j^{(1)}, \quad (19)$$

and it multiplies σ^B . The NLL terms are in general not all proportional to σ^B . The coefficient c_2 is defined by $c_2 = c_2^\mu + T_2$, with $c_2^\mu = -\sum_i A_i^{(1)} \ln(\mu_F^2/m_t^2)$ denoting the terms involving logarithms of the scale, and

$$\begin{aligned} T_2 = & \sum_i \left[-2 A_i^{(1)} \ln \left(\frac{-t_i}{m_t^2} \right) + D_i^{(1)} - A_i^{(1)} \ln \left(\frac{m_t^2}{s} \right) \right] \\ & + \sum_j \left[B_j^{(1)} + D_j^{(1)} - A_j^{(1)} \ln \left(\frac{m_t^2}{s} \right) \right], \end{aligned} \quad (20)$$

where t_i stands for $t - m_t^2$ or $u - m_t^2$, while A^c is defined by

$$A^c = \text{tr} \left(H^{(0)} \Gamma_S^{(1)\dagger} S^{(0)} + H^{(0)} S^{(0)} \Gamma_S^{(1)} \right). \quad (21)$$

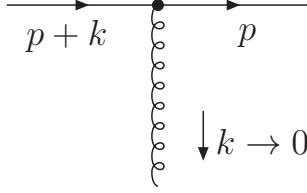


Figure 1: Eikonal diagram for soft-gluon emission from a quark.

The NNLO soft-gluon corrections from the expansion of the resummed cross section are

$$\begin{aligned} \hat{\sigma}^{(2)} = & \sigma^B \frac{\alpha_s^2(\mu_R)}{\pi^2} \left\{ \frac{1}{2} c_3^2 \mathcal{D}_3(s_4) + \left[\frac{3}{2} c_3 c_2 - \frac{\beta_0}{4} c_3 + \sum_j \frac{\beta_0}{8} A_j^{(1)} \right] \mathcal{D}_2(s_4) + \dots \right\} \\ & + \frac{\alpha_s^{d_{\alpha_s}+2}(\mu_R)}{\pi^2} \left\{ \frac{3}{2} c_3 A^c \mathcal{D}_2(s_4) + \dots \right\} \end{aligned} \quad (22)$$

where for brevity we do not show further subleading terms.

The N³LO soft-gluon corrections from the expansion of the resummed cross section are

$$\begin{aligned} \hat{\sigma}^{(3)} = & \sigma^B \frac{\alpha_s^3(\mu_R)}{\pi^3} \left\{ \frac{1}{8} c_3^3 \mathcal{D}_5(s_4) + \left[\frac{5}{8} c_3^2 c_2 - \frac{5}{24} c_3^2 \beta_0 + \frac{5}{48} c_3 \beta_0 \sum_j A_j^{(1)} \right] \mathcal{D}_4(s_4) + \dots \right\} \\ & + \frac{\alpha_s^{d_{\alpha_s}+3}(\mu_R)}{\pi^3} \left\{ \frac{5}{8} c_3^2 A^c \mathcal{D}_4(s_4) + \dots \right\} \end{aligned} \quad (23)$$

where, again for brevity, we do not show further subleading terms.

Results for PIM kinematics are analogous: we replace $D_k(s_4)$ by $D_k(1-z)$ and drop terms involving the t_i variables in the above expressions.

3 Soft anomalous dimensions in top-pair production

3.1 Cusp anomalous dimension

The Feynman rules for diagrams with soft gluon emission simplify in the eikonal approximation (see Fig. 1), as

$$\begin{aligned} & \bar{u}(p) (-ig_s T_F^c) \gamma^\mu \frac{i(\not{p} + \not{k} + m)}{(p+k)^2 - m^2 + i\epsilon} \\ & \rightarrow \bar{u}(p) g_s T_F^c \gamma^\mu \frac{\not{p} + m}{2p \cdot k + i\epsilon} = \bar{u}(p) g_s T_F^c \frac{v^\mu}{v \cdot k + i\epsilon} \end{aligned} \quad (24)$$

where \bar{u} is a Dirac spinor, T_F^c are the generators of SU(3), and $p^\mu = (\sqrt{s}/2)v^\mu$.

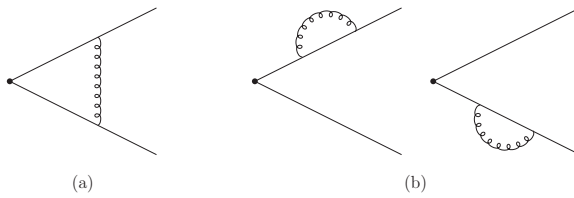


Figure 2: One-loop vertex (left) and self-energy (right) eikonal diagrams for the cusp anomalous dimension.

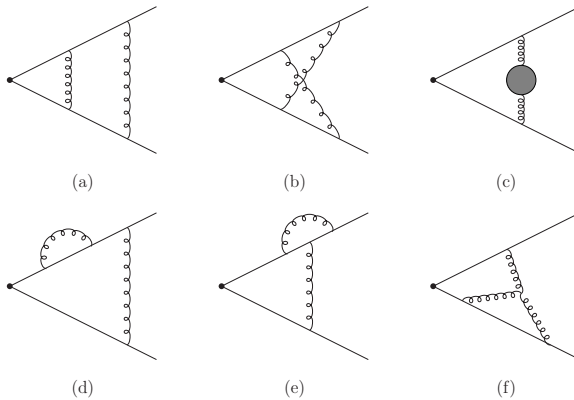


Figure 3: Two-loop vertex diagrams for the cusp anomalous dimension.

We begin with the massive cusp anomalous dimension [35], which is the simplest soft anomalous dimension and an essential component of calculations for top-quark production. Calculations can be performed in momentum space and in Feynman gauge, although other choices are possible.

The one-loop diagrams for the cusp anomalous dimension, with eikonal lines representing the top and the antitop quarks, are shown in Fig. 2. The left graph (a) is the one-loop vertex correction, while the graph on the right (b) shows the one-loop top and antitop self-energy diagrams.

The one-loop cusp anomalous dimension, $\Gamma_{\text{cusp}}^{(1)}$, is found from the coefficient of the ultraviolet pole of the one-loop diagrams [35]:

$$\Gamma_{\text{cusp}}^{(1)} = C_F \left[-\frac{(1 + \beta^2)}{2\beta} \ln \left(\frac{1 - \beta}{1 + \beta} \right) - 1 \right] \quad (25)$$

where, as before, $\beta = \sqrt{1 - 4m_t^2/s}$.

In terms of the cusp angle θ [100], where $\theta = \cosh^{-1}(v_i \cdot v_j / \sqrt{v_i^2 v_j^2}) = \ln[(1 + \beta)/(1 - \beta)]$, or $\beta = \tanh(\theta/2)$, we can rewrite the one-loop expression as

$$\Gamma_{\text{cusp}}^{(1)} = C_F(\theta \coth \theta - 1). \quad (26)$$

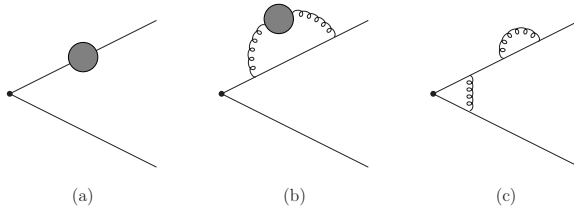


Figure 4: Two-loop top-quark self-energy graphs.

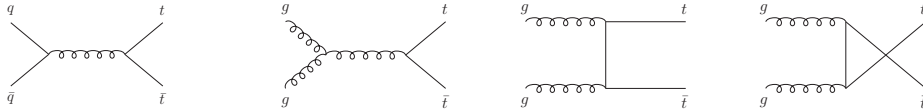


Figure 5: Lowest-order diagrams for the $q\bar{q} \rightarrow t\bar{t}$ channel (left diagram) and the $g g \rightarrow t\bar{t}$ channel (right three diagrams).

At two loops, the vertex-correction graphs for the cusp anomalous dimension are shown in Fig. 3 while the top-quark self-energy graphs are shown in Fig. 4. The grey blobs in the diagrams represent quark, gluon, and ghost loops.

With the inclusion of counterterms and after multiplying with the relevant color factors, the two-loop cusp anomalous dimension, as determined from the ultraviolet poles, is [35]:

$$\begin{aligned} \Gamma_{\text{cusp}}^{(2)} = & \frac{K}{2} \Gamma_{\text{cusp}}^{(1)} + C_F C_A \left\{ \frac{1}{2} + \frac{\zeta_2}{2} + \frac{\theta^2}{2} \right. \\ & \left. - \frac{1}{2} \coth^2 \theta \left[\zeta_3 - \zeta_2 \theta - \frac{\theta^3}{3} - \theta \text{Li}_2(e^{-2\theta}) - \text{Li}_3(e^{-2\theta}) \right] \right. \\ & \left. - \frac{1}{2} \coth \theta \left[\zeta_2 + \zeta_2 \theta + \theta^2 + \frac{\theta^3}{3} + 2\theta \ln(1 - e^{-2\theta}) - \text{Li}_2(e^{-2\theta}) \right] \right\} \quad (27) \end{aligned}$$

where $\zeta_3 = 1.2020569 \dots$.

An excellent approximation to the complete two-loop result that is valid for all β is given by [35]:

$$\Gamma_{\text{cusp approx}}^{(2)} = \frac{K}{2} \Gamma_{\text{cusp}}^{(1)} + C_F C_A \left(1 - \frac{2}{3} \zeta_2 \right) \beta^2. \quad (28)$$

The complete three-loop result $\Gamma_{\text{cusp}}^{(3)}$ is very long [101, 102]. A very simple but excellent numerical approximation, for $n_f = 5$, that is valid for all β is given by [102]

$$\Gamma_{\text{cusp approx}}^{(3)} = 2.80322 \Gamma_{\text{cusp}}^{(1)} + 0.09221 \beta^2. \quad (29)$$

3.2 Soft anomalous dimension matrices for $t\bar{t}$ production

The top-antitop pair production partonic processes at lowest order are

$$q(p_1) + \bar{q}(p_2) \rightarrow t(p_3) + \bar{t}(p_4) \quad (30)$$

and

$$g(p_1) + g(p_2) \rightarrow t(p_3) + \bar{t}(p_4). \quad (31)$$

The diagrams for these processes are shown in Fig. 5. We define $s = (p_1 + p_2)^2$, $t_1 = (p_1 - p_3)^2 - m_t^2$, and $u_1 = (p_2 - p_3)^2 - m_t^2$.

Next, we present the one-loop and two-loop results for the soft anomalous matrices for these partonic processes. The soft anomalous dimension matrix for $q(p_1) + \bar{q}(p_2) \rightarrow t(p_3) + \bar{t}(p_4)$ in a color tensor basis of s -channel singlet and octet exchange,

$$c_1 = \delta_{12}\delta_{34}, \quad c_2 = T_{F\ 21}^c T_{F\ 34}^c, \quad (32)$$

can be written as

$$\Gamma_S^{q\bar{q} \rightarrow t\bar{t}} = \begin{bmatrix} \Gamma_{11}^{q\bar{q}} & \Gamma_{12}^{q\bar{q}} \\ \Gamma_{21}^{q\bar{q}} & \Gamma_{22}^{q\bar{q}} \end{bmatrix}. \quad (33)$$

At one loop we have [13, 17, 60]

$$\begin{aligned} \Gamma_{11}^{q\bar{q}(1)} &= \Gamma_{\text{cusp}}^{(1)} \\ \Gamma_{12}^{q\bar{q}(1)} &= \frac{C_F}{C_A} \ln\left(\frac{t_1}{u_1}\right) \\ \Gamma_{21}^{q\bar{q}(1)} &= 2 \ln\left(\frac{t_1}{u_1}\right) \\ \Gamma_{22}^{q\bar{q}(1)} &= \left(1 - \frac{C_A}{2C_F}\right) \Gamma_{\text{cusp}}^{(1)} + 4C_F \ln\left(\frac{t_1}{u_1}\right) - \frac{C_A}{2} \left[1 + \ln\left(\frac{sm_t^2 t_1^2}{u_1^4}\right)\right]. \end{aligned} \quad (34)$$

At two loops we have [49, 60]

$$\begin{aligned} \Gamma_{11}^{q\bar{q}(2)} &= \Gamma_{\text{cusp}}^{(2)} \\ \Gamma_{12}^{q\bar{q}(2)} &= \left(\frac{K}{2} - \frac{C_A}{2} N_{2l}\right) \Gamma_{12}^{q\bar{q}(1)} \\ \Gamma_{21}^{q\bar{q}(2)} &= \left(\frac{K}{2} + \frac{C_A}{2} N_{2l}\right) \Gamma_{21}^{q\bar{q}(1)} \\ \Gamma_{22}^{q\bar{q}(2)} &= \frac{K}{2} \Gamma_{22}^{q\bar{q}(1)} + \left(1 - \frac{C_A}{2C_F}\right) \left(\Gamma_{\text{cusp}}^{(2)} - \frac{K}{2} \Gamma_{\text{cusp}}^{(1)}\right). \end{aligned} \quad (35)$$

Here N_{2l} is given by

$$N_{2l} = \frac{\theta^2}{2} - \frac{1}{2} \coth \theta \left[\theta^2 + 2\theta \ln(1 - e^{-2\theta}) - \text{Li}_2(e^{-2\theta}) \right]. \quad (36)$$

The soft anomalous dimension matrix for $g(p_1) + g(p_2) \rightarrow t(p_3) + \bar{t}(p_4)$ in a color tensor basis

$$c_1 = \delta^{12} \delta_{34}, \quad c_2 = d^{12c} T_{34}^c, \quad c_3 = if^{12c} T_{34}^c \quad (37)$$

where d and f are the totally symmetric and antisymmetric $SU(3)$ tensors, is

$$\Gamma_S^{gg \rightarrow t\bar{t}} = \begin{bmatrix} \Gamma_{11}^{gg} & 0 & \Gamma_{13}^{gg} \\ 0 & \Gamma_{22}^{gg} & \Gamma_{23}^{gg} \\ \Gamma_{31}^{gg} & \Gamma_{32}^{gg} & \Gamma_{22}^{gg} \end{bmatrix}. \quad (38)$$

At one loop we have [17, 60]

$$\begin{aligned}
\Gamma_{11}^{gg(1)} &= \Gamma_{\text{cusp}}^{(1)} \\
\Gamma_{13}^{gg(1)} &= \ln\left(\frac{t_1}{u_1}\right) \\
\Gamma_{31}^{gg(1)} &= 2 \ln\left(\frac{t_1}{u_1}\right) \\
\Gamma_{22}^{gg(1)} &= \left(1 - \frac{C_A}{2C_F}\right) \Gamma_{\text{cusp}}^{(1)} - \frac{C_A}{2} \left[1 + \ln\left(\frac{sm_t^2}{t_1 u_1}\right)\right] \\
\Gamma_{23}^{gg(1)} &= \frac{C_A}{2} \ln\left(\frac{t_1}{u_1}\right) \\
\Gamma_{32}^{gg(1)} &= \frac{(N_c^2 - 4)}{2N_c} \ln\left(\frac{t_1}{u_1}\right)
\end{aligned} \tag{39}$$

At two loops we find [49, 60]

$$\begin{aligned}
\Gamma_{11}^{gg(2)} &= \Gamma_{\text{cusp}}^{(2)} \\
\Gamma_{13}^{gg(2)} &= \left(\frac{K}{2} - \frac{C_A}{2} N_{2l}\right) \Gamma_{13}^{gg(1)} \\
\Gamma_{31}^{gg(2)} &= \left(\frac{K}{2} + \frac{C_A}{2} N_{2l}\right) \Gamma_{31}^{gg(1)} \\
\Gamma_{22}^{gg(2)} &= \frac{K}{2} \Gamma_{22}^{gg(1)} + \left(1 - \frac{C_A}{2C_F}\right) \left(\Gamma_{\text{cusp}}^{(2)} - \frac{K}{2} \Gamma_{\text{cusp}}^{(1)}\right) \\
\Gamma_{23}^{gg(2)} &= \frac{K}{2} \Gamma_{23}^{gg(1)} \\
\Gamma_{32}^{gg(2)} &= \frac{K}{2} \Gamma_{32}^{gg(1)}
\end{aligned} \tag{40}$$

4 Top-antitop pair production

4.1 Total cross sections for $t\bar{t}$ production

We begin our presentation of numerical results with the total cross section for top-antitop pair production. The total hadronic cross section is calculated by integrating over the convolution of the double-differential partonic cross section with the parton distribution functions ϕ .

We denote the NLO soft-gluon corrections from the expansion of the NNLL resummed cross section as approximate NLO (aNLO) corrections. Similarly the NNLO soft-gluon corrections are denoted as approximate NNLO (aN²LO) corrections, and the N³LO soft-gluon corrections are denoted as approximate N³LO (aN³LO) corrections. The aNLO and aN²LO corrections are extremely good approximations to the exact NLO and NNLO results, respectively, for total cross sections as well as top-quark differential distributions at all Tevatron and LHC energies (see e.g. the discussion in Ref. 60). The best aN³LO prediction is given by the sum of the NNLO cross section and the aN³LO soft-gluon corrections.

Collider Energy	Cross section \pm scale \pm pdf
1.8 TeV $p\bar{p}$	$6.130^{+0.076+0.179}_{-0.233-0.160}$
1.96 TeV $p\bar{p}$	$7.876^{+0.096+0.224}_{-0.293-0.203}$
5.02 TeV pp	$71.3^{+2.2+1.9}_{-3.3-2.8}$
7 TeV pp	$183.0^{+5.4+4.0}_{-6.9-5.6}$
8 TeV pp	$260.1^{+7.4+5.3}_{-8.6-7.3}$
13 TeV pp	$842.5^{+25.3+13.7}_{-16.9-17.7}$
14 TeV pp	$995.0^{+29.7+15.7}_{-19.0-20.2}$

Table 1: aN³LO top-antitop production cross sections [61] with $m_t = 172.5$ GeV at LHC pp and Tevatron $p\bar{p}$ collider energies.

A comparison of various approximate predictions using higher-order soft-gluon corrections, all made before the exact NNLO cross section was known, is shown in Fig. 6, all with the same choice of parameters and MSTW2008 [103] pdf, at 1.96 TeV Tevatron energy and at 7, 8, and 14 TeV LHC energies. Moreover, exact NLO and NNLO results for the total cross sections are also shown on the plot. We observe the success or lack thereof of the various predictions in predicting the exact NNLO result.

Ref. [49] uses the QCD moment-space resummation formalism for the double-differential cross section. Ref. [47] uses QCD moment-space resummation with absolute threshold for the total-only cross section. Ref. [44] uses the SCET resummation formalism for the double-differential cross section, while Ref. [54] uses SCET resummation with absolute threshold for the total-only cross section. Lastly, Ref. [55] uses QCD moment-space resummation with absolute threshold for the total-only cross section.

The result in Ref. [49] is very close to the exact NNLO [88] result: the central values and the scale uncertainty are nearly identical, for all collider energies, with less than 1% difference between approximate and exact cross sections. This was expected from the comparison of approximate NNLO results in different kinematics in Ref. [27] (see also the discussions in [49] and [60]).

In Fig. 7 we display theoretical predictions at aN³LO [61] for the total cross section as a function of top-quark mass at the LHC and the Tevatron. We use MMHT2014 [104] NNLO pdf but note that the results with CT14 [105] and NNPDF [106] pdf are very similar. We compare the aN³LO results with data from the LHC at 5.02 TeV [107], 7 TeV [108,109], 8 TeV [109,110], and 13 TeV [111,112], and from the Tevatron at 1.8 TeV [113,114] and 1.96 TeV [115]. We find superb agreement between the theoretical predictions and the data.

In Table 1 we present the aN³LO cross sections [61] for $t\bar{t}$ production. The central result at each energy is with $\mu_F = \mu_R = m_t$, the first uncertainty is from independent variation of μ_F and μ_R over the range $m_t/2$ to $2m_t$, and the second uncertainty is from the MMHT2014 [104] NNLO pdf.

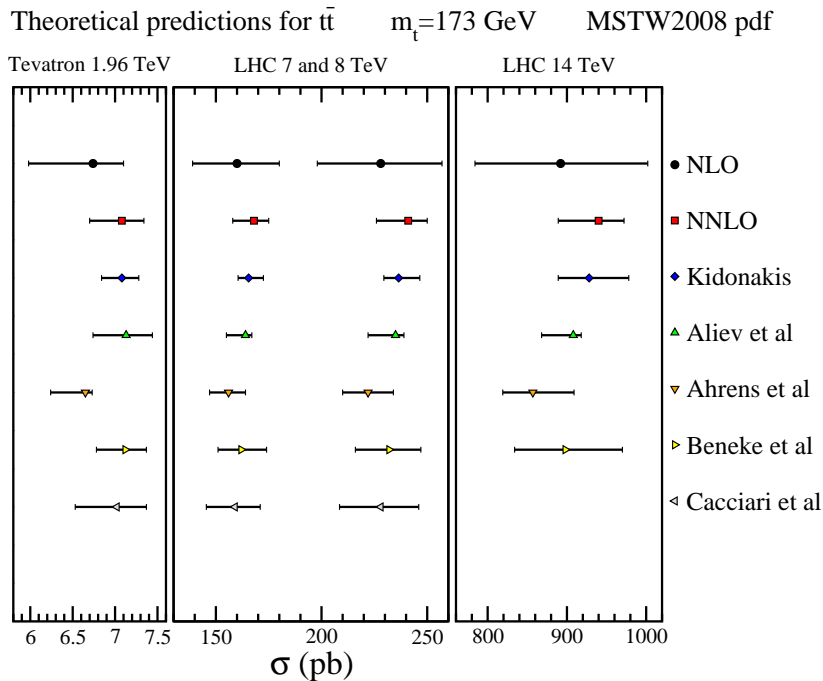


Figure 6: Theoretical predictions with soft-gluon corrections [47, 49, 52, 54, 55] from 2010 and 2011 compared to NLO and NNLO results for Tevatron and LHC energies.

4.2 Top-quark p_T and rapidity distributions in $t\bar{t}$ production

We continue with top quark differential distributions in $t\bar{t}$ production. We present theoretical results for the top-quark transverse momentum and rapidity distributions at Tevatron and LHC energies.

The aN³LO top-quark p_T distributions [64], with scales $\mu = m_t/2$, m_t , and $2m_t$, and $m_t = 172.5$ GeV, are displayed in Fig. 8 at 7, 8, 13, and 14 TeV LHC energies.

The left plot in Fig. 9 shows the aN³LO top-quark normalized p_T distribution, $(1/\sigma)d\sigma/dp_T$, at the LHC compared to CMS [116] data at 13 TeV energy. Two different choices of scale are used, $\mu = m_t$ and $\mu = m_T$, where $m_T = \sqrt{p_T^2 + m_t^2}$. There is excellent agreement with data. In the right plot of Fig. 9, the aN³LO top-quark normalized p_T distribution at 8 TeV LHC energy with scale m_t and m_T is compared to ATLAS [117] data, again with excellent agreement. The high- p_T region is highlighted in the inset plots.

Figure 10 shows the aN³LO top-quark normalized p_T distribution at the LHC compared to CMS [118] data at 8 TeV energy. There is excellent agreement with data in both the dilepton and lepton+jets channels.

Figure 11 shows the aN³LO boosted-top quark p_T distribution at the LHC compared to ATLAS [119] and CMS [120] data at 8 TeV energy. There is excellent agreement with the data.

The aN³LO top-quark normalized p_T distribution at 7 TeV LHC energy is shown in Fig. 12 and compared with CMS [121] data in the dilepton and lepton+jets channels. We note the excellent agreement of theory with data.

In the left plot of Fig. 13, the aN³LO top-quark normalized p_T distribution at 7 TeV LHC

pp \rightarrow $t\bar{t}$ at LHC energies aN³LO $m_t=172.5$ GeV

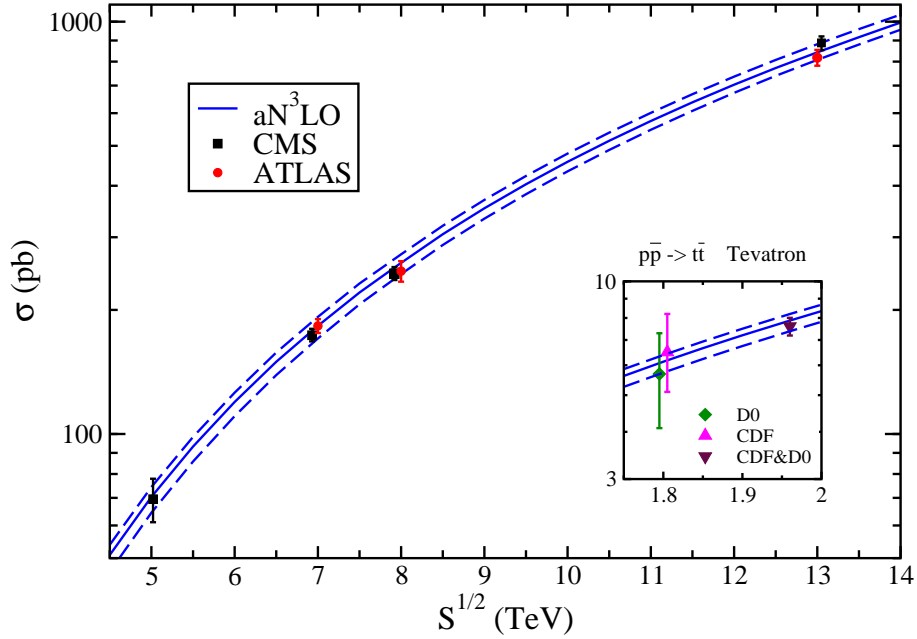


Figure 7: The aN³LO [61] top-antitop pair total cross section, with theoretical uncertainties, as a function of LHC energy, compared with CMS data at 5.02 TeV [107] and with ATLAS and CMS data at 7 TeV [108, 109], 8 TeV [109, 110], and 13 TeV [111, 112] LHC energies. The inset plot shows the aN³LO cross section at Tevatron energies compared with CDF [113] and D0 [114] data at 1.8 TeV, and CDF&D0 combination [115] at 1.96 TeV.

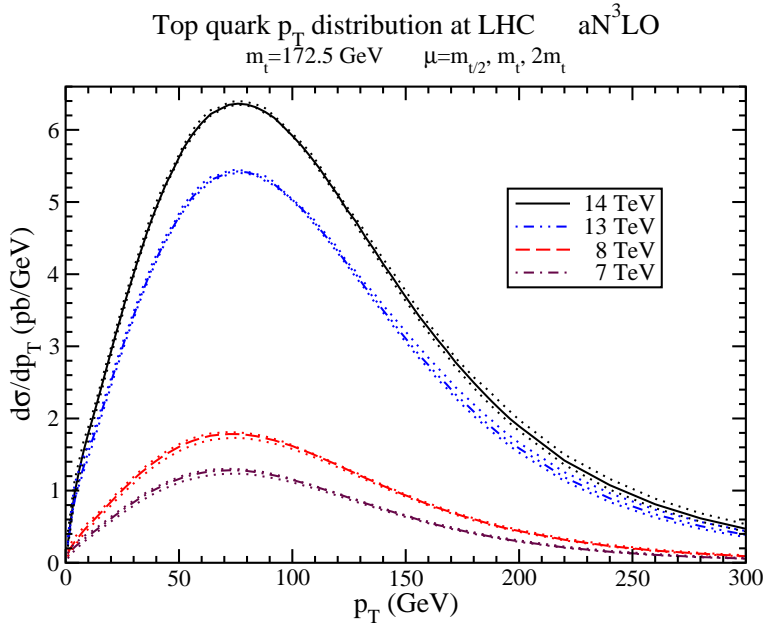


Figure 8: The aN³LO [64] top-quark p_T distributions at 7, 8, 13, and 14 TeV LHC energies.

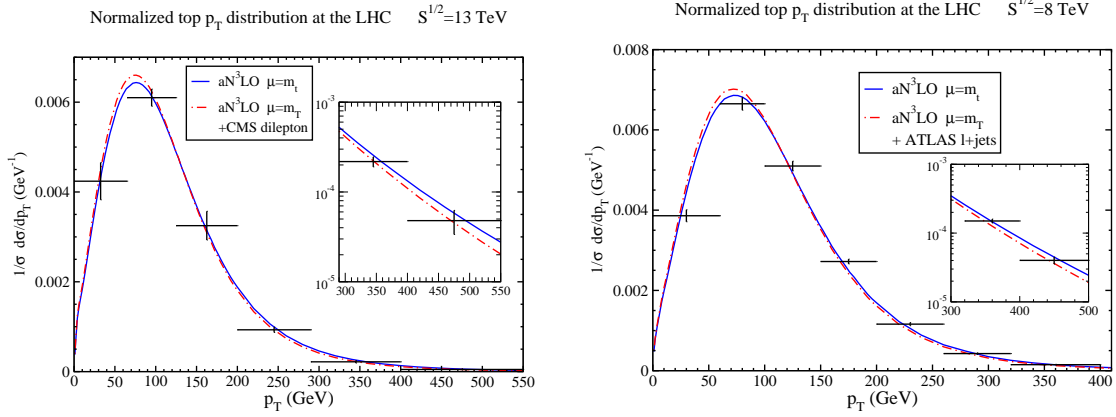


Figure 9: The aN³LO top-quark normalized p_T distribution (left) at 13 TeV LHC energy compared with CMS [116] data and (right) at 8 TeV energy compared with ATLAS [117] lepton+jets data.

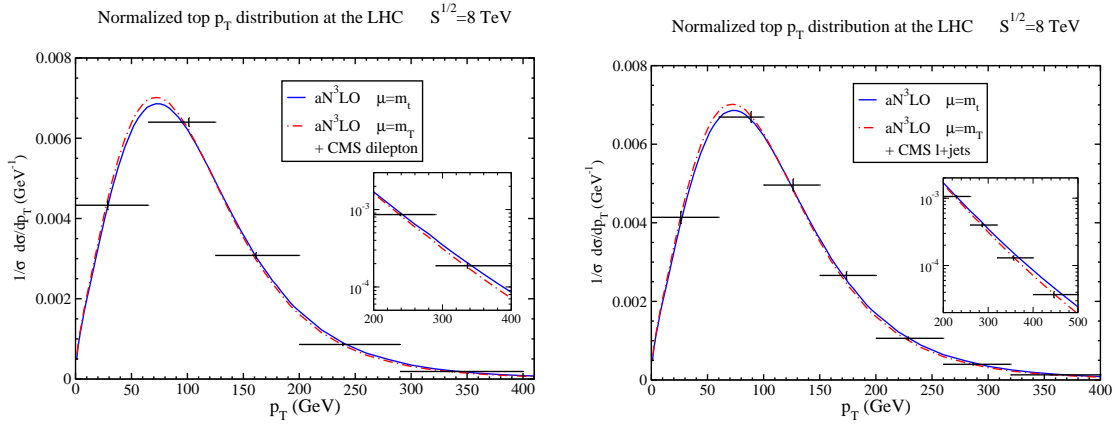


Figure 10: The aN³LO top-quark normalized p_T distribution at 8 TeV LHC energy compared with CMS [118] dilepton (left) and lepton+jets (right) data.

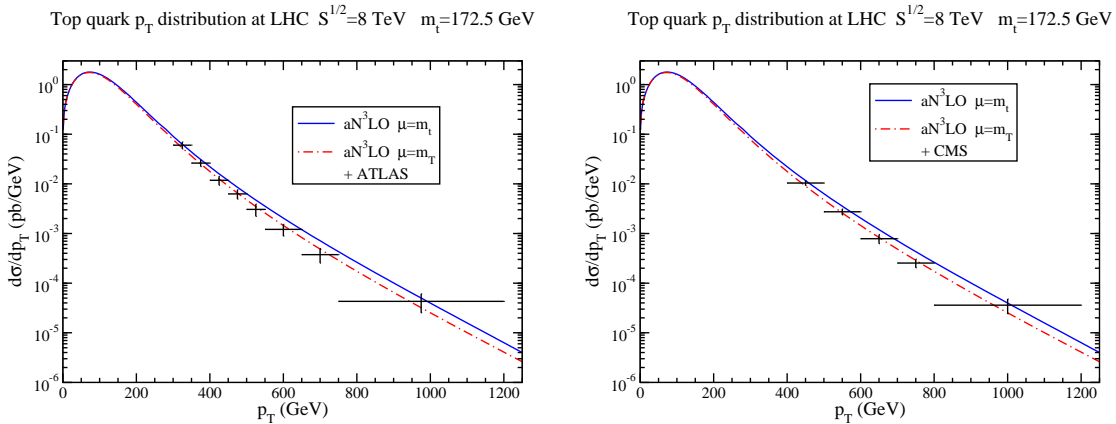


Figure 11: The aN³LO top-quark p_T distribution at 8 TeV LHC energy compared with ATLAS [119] (left) and CMS [120] (right) data.

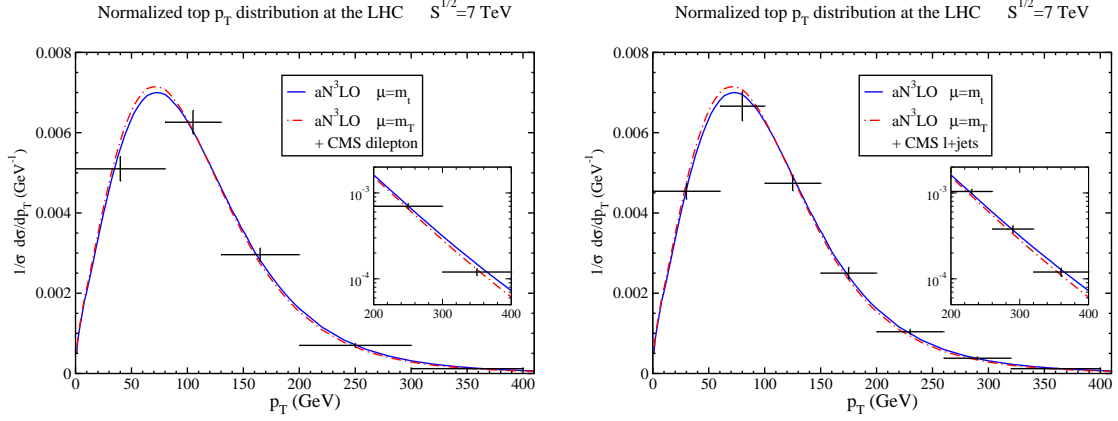


Figure 12: The aN³LO top-quark normalized p_T distribution at 7 TeV LHC energy compared with CMS [121] dilepton (left) and lepton+jets (right) data.

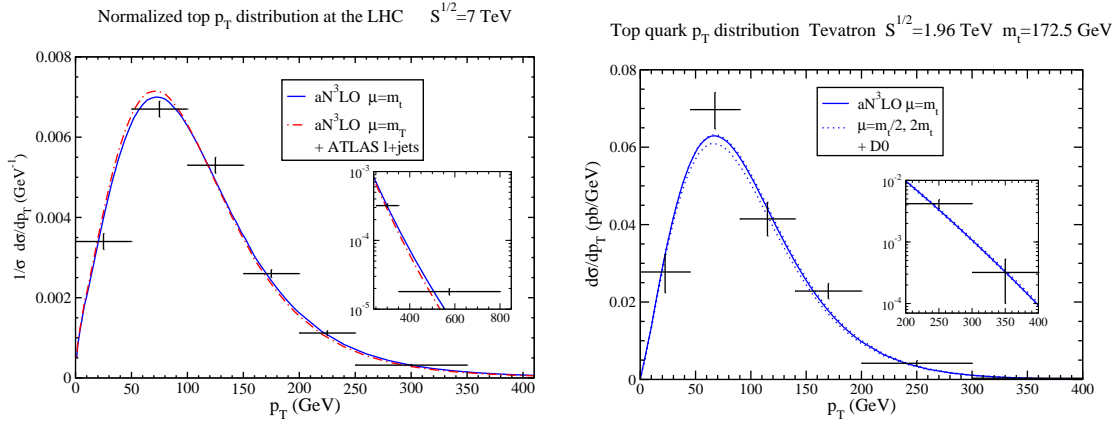


Figure 13: (Left) The aN³LO top-quark normalized p_T distribution at 7 TeV LHC energy compared with ATLAS [122] lepton+jets data. (Right) The aN³LO top-quark p_T distribution at 1.96 TeV Tevatron energy compared with data from D0 [123].

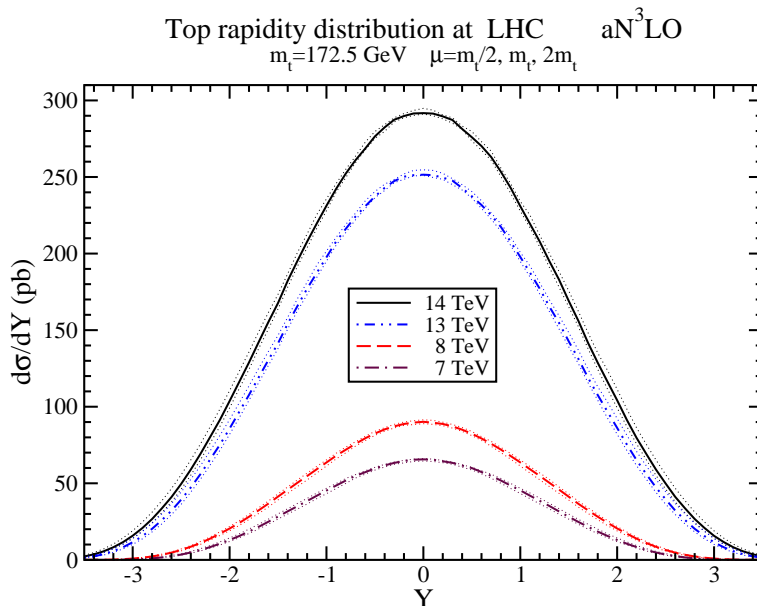


Figure 14: The aN³LO [64] top-quark rapidity distributions at 7, 8, 13, and 14 TeV LHC energies.

energy is compared to ATLAS [122] data. The right plot of Fig. 13 displays the aN³LO top quark p_T distribution at 1.96 TeV Tevatron energy. Excellent agreement of the aN³LO results with D0 data [123] can be seen, including the high- p_T region shown in the inset.

The aN³LO top-quark rapidity distributions at 7, 8, 13, and 14 TeV LHC energies are displayed in Fig. 14 with scale choices $\mu = m_t/2, m_t,$ and $2m_t$.

The aN³LO top-quark normalized rapidity distribution, $(1/\sigma)d\sigma/dY$, at 13 TeV LHC energy is shown in the left plot of Fig. 15 and compared with CMS [116] data. In the right plot of Fig. 15, the aN³LO top-quark normalized absolute value rapidity distribution at 8 TeV LHC energy is compared to ATLAS [117] data. We find excellent agreement between theory and data in both cases.

The aN³LO top-quark normalized rapidity distribution at 8 TeV LHC energy is shown in Fig. 16 and compared with CMS [118] dilepton and lepton+jets data, again with excellent agreement.

The aN³LO top-quark normalized rapidity distribution at 7 TeV LHC energy is shown in Fig. 17 and compared with CMS [121] dilepton and lepton+jets data. We again note the excellent agreement between theory and data.

The aN³LO top-quark rapidity distribution has been calculated for 1.96 TeV Tevatron energy as shown in the left plot in Fig. 18, and it is in very good agreement with data from D0 [123].

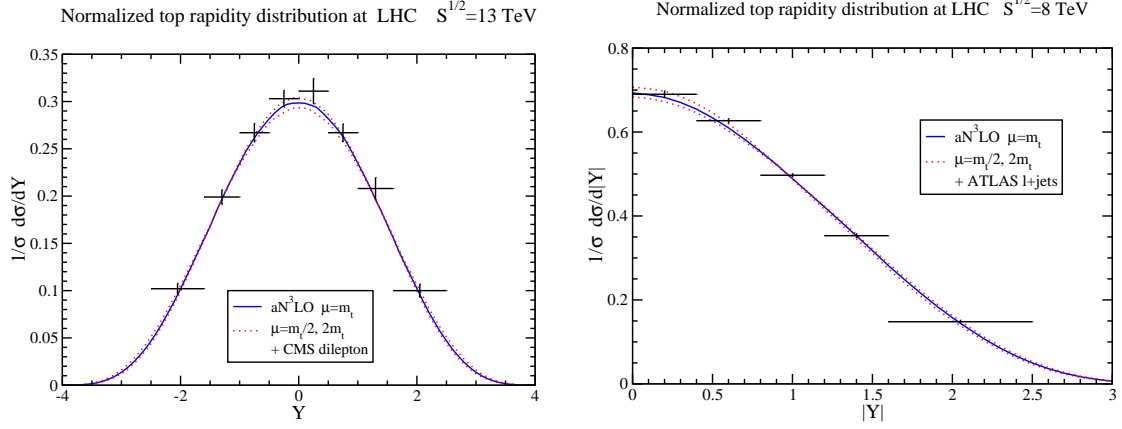


Figure 15: (Left) The aN^3LO top-quark normalized rapidity distribution at 13 TeV LHC energy compared with CMS data [116]. (Right) The aN^3LO top-quark normalized absolute value rapidity distribution at 8 TeV LHC energy compared with ATLAS [117] data.

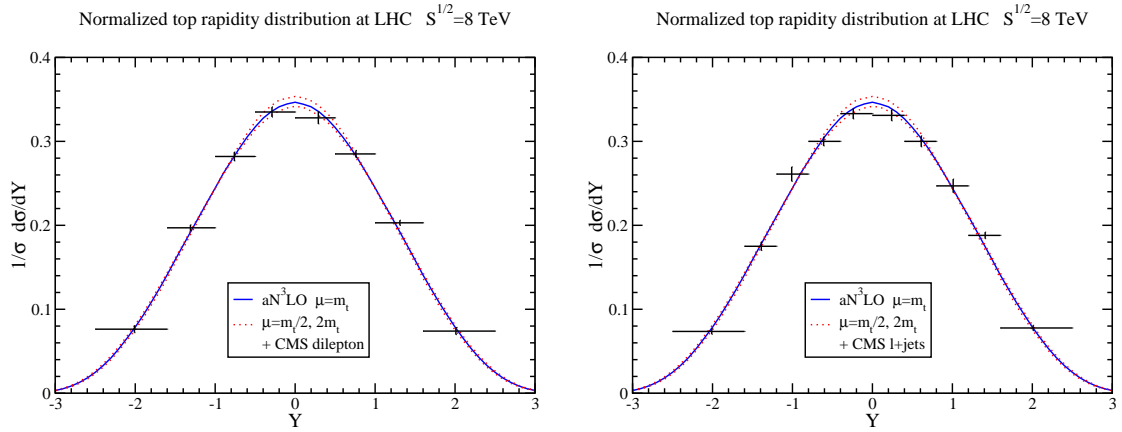


Figure 16: The aN^3LO top-quark normalized rapidity distribution at 8 TeV LHC energy compared with CMS [118] dilepton (left) and lepton+jets (right) data.

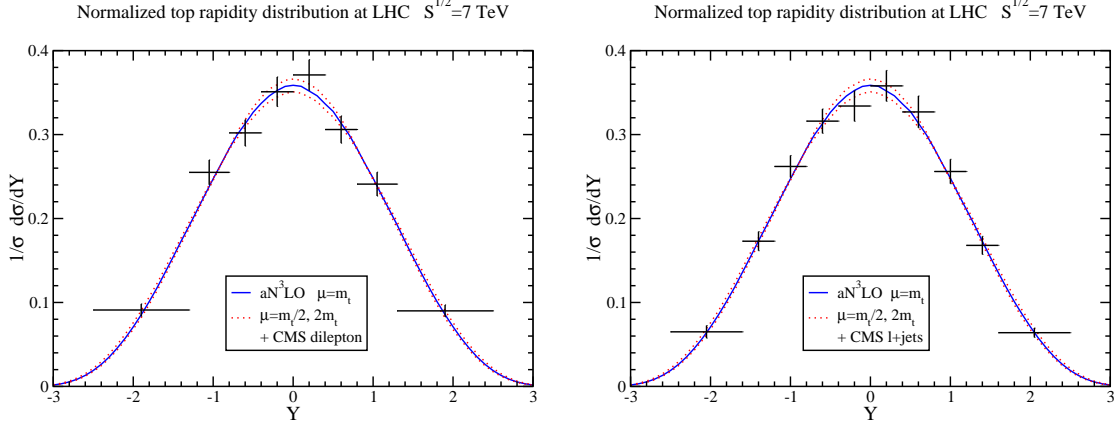


Figure 17: The aN³LO top-quark normalized rapidity distribution at 7 TeV LHC energy compared with CMS [121] dilepton (left) and lepton+jets (right) data.

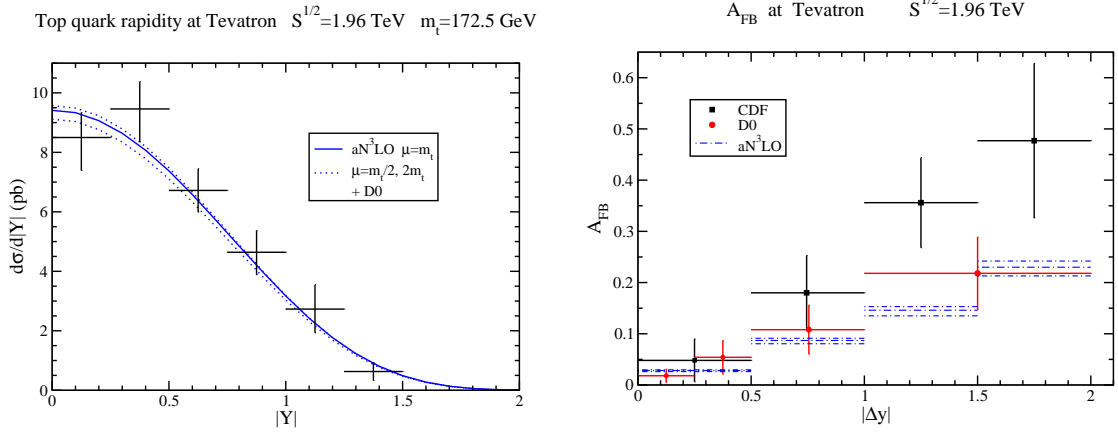


Figure 18: (Left) The aN³LO top-quark rapidity distribution at 1.96 TeV Tevatron energy compared with D0 [123] data. (Right) The aN³LO differential forward-backward asymmetry at 1.96 Tevatron energy compared with D0 [130] and CDF [131] data.

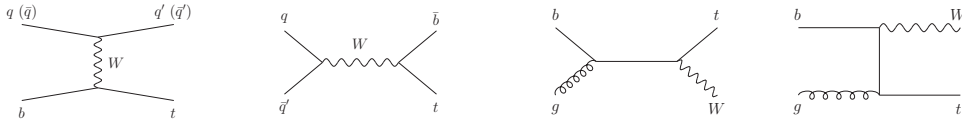


Figure 19: Lowest-order diagrams for single-top production in the t -channel (left diagram), s -channel (second from left), and in tW production (right two diagrams).

4.3 Top-quark forward-backward asymmetry

The top-quark forward-backward asymmetry is defined by

$$A_{\text{FB}} = \frac{\sigma(Y > 0) - \sigma(Y < 0)}{\sigma(Y > 0) + \sigma(Y < 0)}. \quad (41)$$

The asymmetry is very significant at the Tevatron. In addition to QCD corrections, electroweak corrections are important for this asymmetry [124–127] (see also Ref. [128] for rapidity distributions at the LHC). The theoretical result at aN³LO and including electroweak corrections for 1.96 TeV Tevatron energy is [65] $A_{\text{FB}} = 0.100 \pm 0.006$ which is in agreement with the CDF and D0 combination [129] of 0.128 ± 0.025 . The aN³LO differential A_{FB} is plotted in the right plot of Fig. 18 and compared with D0 [130] and CDF [131] data.

5 Single-top production

Collider Energy	t -channel t	t -channel \bar{t}	t -channel t and \bar{t}	s -channel t	s -channel \bar{t}	s -channel t and \bar{t}	tW^-
1.96 TeV $p\bar{p}$	1.088	1.088	2.176	0.52	0.52	1.04	0.102
7 TeV pp	43.9	23.7	67.6	3.21	1.56	4.77	8.5
8 TeV pp	57.5	31.7	89.2	3.86	1.96	5.82	12.0
13 TeV pp	139.6	84.0	223.6	7.29	4.20	11.49	38.1
14 TeV pp	158.3	96.1	254.3	7.98	4.68	12.66	44.8

Table 2: aNNLO t -channel [73] and s -channel [70] single-top, single-antitop, and combined cross sections, and aN³LO tW^- [77] cross sections with $m_t = 172.5$ GeV at LHC pp and Tevatron $p\bar{p}$ collider energies.

Single-top-quark production was first observed at the Tevatron in 2009 [3,4]. The single-top partonic processes at lowest order are shown in Fig. 19.

The t -channel partonic processes are of the form $qb \rightarrow q't$ and $\bar{q}b \rightarrow \bar{q}'t$ and are numerically the largest among single-top processes at Tevatron and LHC energies. The s -channel partonic processes are of the form $q\bar{q}' \rightarrow \bar{b}t$ and are numerically second largest at the Tevatron and the smallest at the LHC among single-top processes. The associated tW production proceeds via $bg \rightarrow tW^-$ and is negligible at the Tevatron but second largest numerically among single-top processes at the LHC.

Table 2 summarizes the central values of the cross sections for the various single-top channels at LHC and Tevatron energies.

5.1 t -channel production

We start with single-top production in the t -channel.

The soft anomalous dimension matrix for t -channel single-top production is a 2×2 matrix, and it has been calculated at one loop in Refs. 68,73 and at two loops in Ref. 73. The elements of this matrix are given at one-loop by [68, 73]

$$\begin{aligned}
\Gamma_{S11}^{t(1)} &= C_F \left[\ln \left(\frac{t(t - m_t^2)}{m_t s^{3/2}} \right) - \frac{1}{2} \right] \\
\Gamma_{S12}^{t(1)} &= \frac{C_F}{2N} \ln \left(\frac{u(u - m_t^2)}{s(s - m_t^2)} \right) \\
\Gamma_{S21}^{t(1)} &= \ln \left(\frac{u(u - m_t^2)}{s(s - m_t^2)} \right) \\
\Gamma_{S22}^{t(1)} &= C_F \ln \left(\frac{s - m_t^2}{m_t \sqrt{s}} \right) - \frac{1}{2N} \ln \left(\frac{t(t - m_t^2)}{s(s - m_t^2)} \right) + \frac{(N^2 - 2)}{2N} \ln \left(\frac{u(u - m_t^2)}{s(s - m_t^2)} \right) - \frac{C_F}{2}
\end{aligned} \tag{42}$$

At two loops, the first element of this matrix is given by [73]

$$\Gamma_{S11}^{t(2)} = \frac{K}{2} \Gamma_{S11}^{t(1)} + C_F C_A \frac{(1 - \zeta_3)}{4}. \tag{43}$$

In Figure 20 we plot the aNNLO t -channel single-top and single-antitop cross sections, and their sum, with $m_t = 172.5$ GeV with theoretical uncertainty from scale variation and the pdf error. Excellent agreement is found with D0 and CDF combination [132] at 1.96 TeV energy, and with CMS [133, 135, 138] and ATLAS [134, 136, 137] results at 7, 8, and 13 TeV energies.

The theoretical ratio $\sigma(t)/\sigma(\bar{t}) = 1.85_{-0.08}^{+0.10}$ at 7 TeV compares well with the ATLAS [134] result of 2.04 ± 0.18 . The theoretical ratio $\sigma(t)/\sigma(\bar{t}) = 1.81_{-0.07}^{+0.10}$ at 8 TeV compares well with the ATLAS [136] result of 1.72 ± 0.09 and the CMS [135] result of $1.95 \pm 0.10 \pm 0.19$. The theoretical ratio for the total t -channel cross section $\sigma(8 \text{ TeV})/\sigma(7 \text{ TeV}) = 1.32_{-0.05}^{+0.07}$ compares well with the CMS [135] result of $1.24 \pm 0.08 \pm 0.12$. The theoretical ratio $\sigma(t)/\sigma(\bar{t}) = 1.66_{-0.06}^{+0.08}$ at 13 TeV is in agreement with the ATLAS [137] result of $1.72 \pm 0.09 \pm 0.18$ and the CMS result [138] of $1.81 \pm 0.18 \pm 0.15$.

In addition to the total cross section, the top-quark p_T distribution in t -channel production is of great interest. Figure 21 shows the top (left) and antitop (right) aNNLO p_T distributions in t -channel production at 7 TeV LHC energy together with data from ATLAS [134].

Figure 22 shows the top (left) and antitop (right) aNNLO normalized p_T distributions in t -channel production at 8 TeV LHC energy. We find very good agreement between theory and data from ATLAS [136] for both distributions.

The left plot of Fig. 23 shows the top-quark aNNLO normalized p_T distribution in t -channel production at 8 TeV LHC energy compared to CMS [139] data. We note the very good

Single-top t -channel aNNLO cross sections $m_t=172.5$ GeV

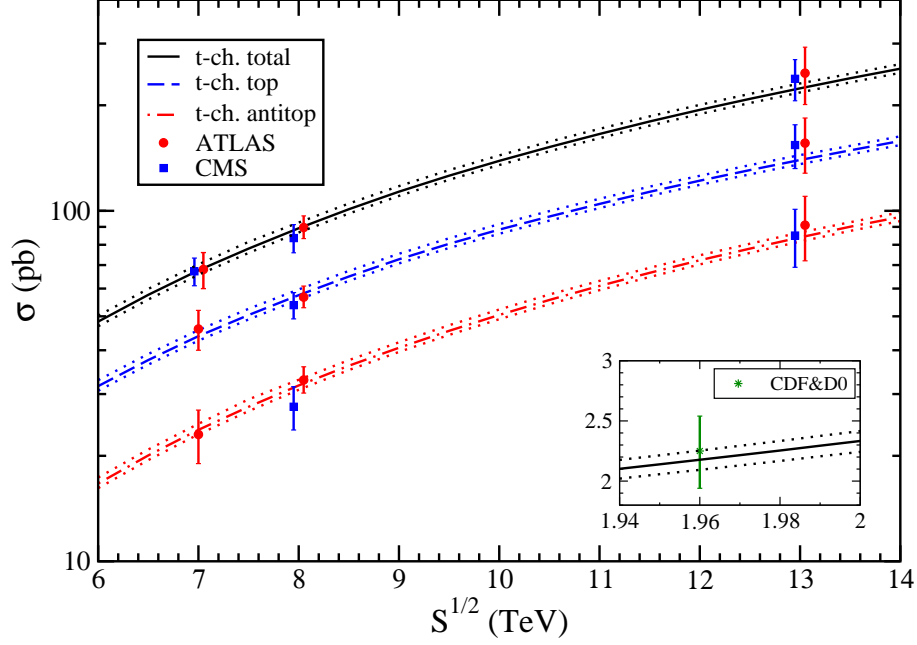


Figure 20: Single-top aNNLO production cross sections in the t -channel compared with (inset) CDF and D0 combination data at 1.96 TeV [132], and with ATLAS and CMS data at 7 TeV [133, 134], 8 TeV [135, 136], and 13 TeV [137, 138].

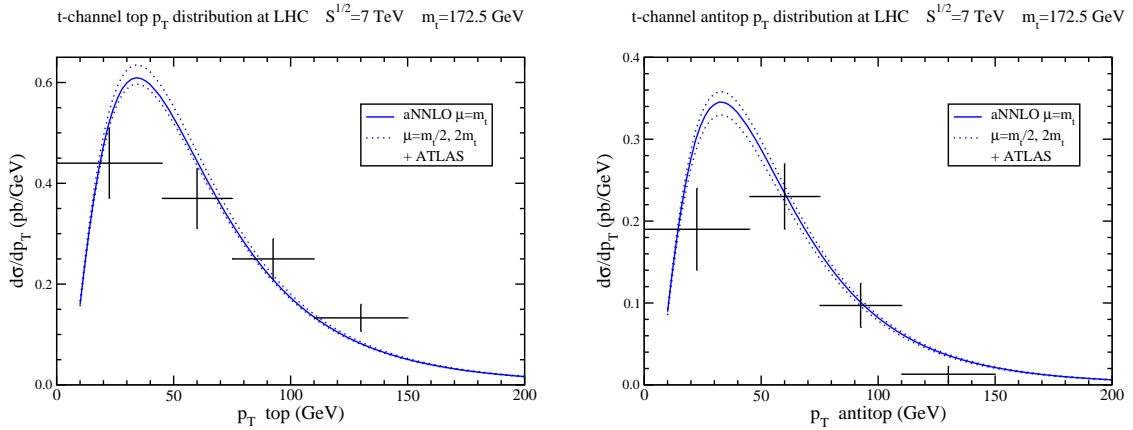


Figure 21: The aNNLO top-quark (left) and antitop (right) p_T distributions in t -channel production at 7 TeV compared to ATLAS [134] data.

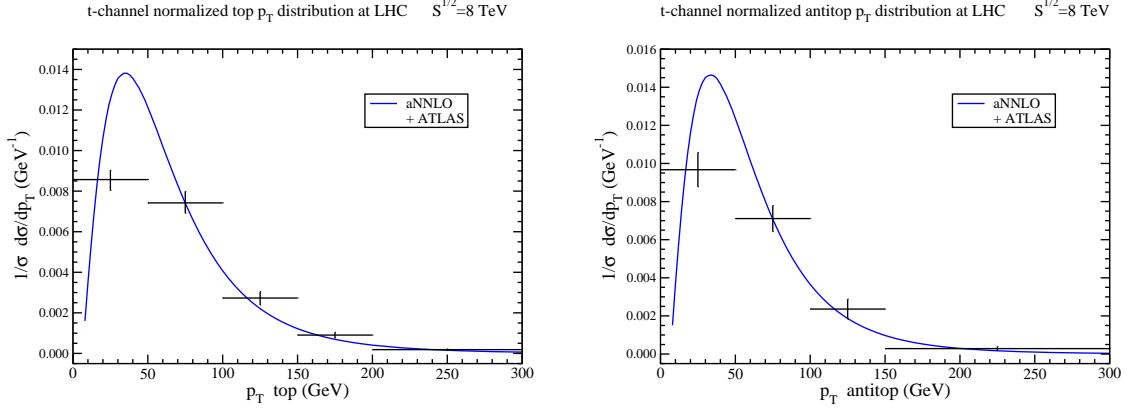


Figure 22: The aNNLO top-quark (left) and antitop (right) normalized p_T distributions in t -channel production at 8 TeV compared to ATLAS [136] data.

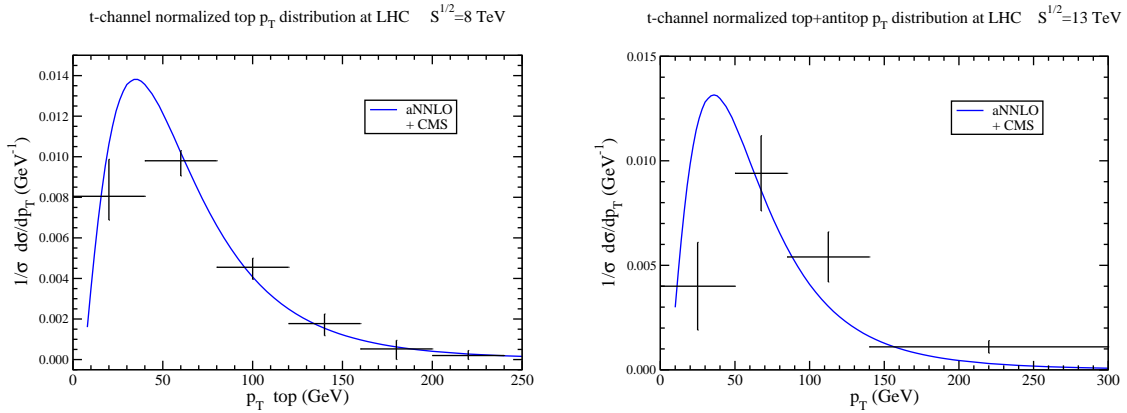


Figure 23: (Left) The aNNLO top-quark normalized p_T distribution in t -channel production at 8 TeV compared to CMS [139] data. (Right) The aNNLO top plus antitop normalized p_T distribution in t -channel production at 13 TeV compared to CMS [140] data.

agreement between theory and data. The plot on the right of Fig. 23 shows the top plus antitop aNNLO normalized p_T distribution in t -channel production at 13 TeV LHC energy compared to CMS [140] data.

5.2 s -channel production

We continue with single-top production in the s -channel.

The soft anomalous dimension matrix for this process has been calculated at one loop [68,70] and at two loops [70]. The 2×2 matrix for s -channel single-top production at one loop is [68,70]

$$\begin{aligned}
\Gamma_{S11}^{s(1)} &= C_F \left[\ln \left(\frac{s - m_t^2}{m_t \sqrt{s}} \right) - \frac{1}{2} \right] \\
\Gamma_{S12}^{s(1)} &= \frac{C_F}{2N} \ln \left(\frac{u(u - m_t^2)}{t(t - m_t^2)} \right) \\
\Gamma_{S21}^{s(1)} &= \ln \left(\frac{u(u - m_t^2)}{t(t - m_t^2)} \right) \\
\Gamma_{S22}^{s(1)} &= C_F \ln \left(\frac{s - m_t^2}{m_t \sqrt{s}} \right) - \frac{1}{N} \ln \left(\frac{u(u - m_t^2)}{t(t - m_t^2)} \right) + \frac{N}{2} \ln \left(\frac{u(u - m_t^2)}{s(s - m_t^2)} \right) - \frac{C_F}{2}
\end{aligned} \tag{44}$$

The first element of this 2×2 matrix at two loops is [70]

$$\Gamma_{S11}^{s(2)} = \frac{K}{2} \Gamma_{S11}^{s(1)} + C_F C_A \frac{(1 - \zeta_3)}{4}. \tag{45}$$

Figure 24 shows the aNNLO cross sections for s -channel production with theoretical uncertainty from scale variation and pdf error. Results are shown for single-top production, single-antitop production, and their sum. Excellent agreement is found with D0 and CDF combination [144], CMS [142], and ATLAS [143] results.

5.3 tW production

We continue with the associated production of a top quark with a W boson. The cross section for $\bar{t}W^+$ production is identical to that for tW^- .

The soft anomalous dimension for $bg \rightarrow tW^-$ is given at one loop by [68,71]

$$\Gamma_S^{tW(1)} = C_F \left[\ln \left(\frac{m_t^2 - t}{m_t \sqrt{s}} \right) - \frac{1}{2} \right] + \frac{C_A}{2} \ln \left(\frac{m_t^2 - u}{m_t^2 - t} \right) \tag{46}$$

and at two loops by [71]

$$\Gamma_S^{tW(2)} = \frac{K}{2} \Gamma_S^{tW(1)} + C_F C_A \frac{(1 - \zeta_3)}{4}. \tag{47}$$

Fig. 25 shows the total tW aN³LO [77] cross section (sum of tW^- and $\bar{t}W^+$) as a function of LHC energy. Excellent agreement is found with data from ATLAS [145] and CMS [146] at

Single-top s -channel aNNLO cross sections $m_t=172.5$ GeV

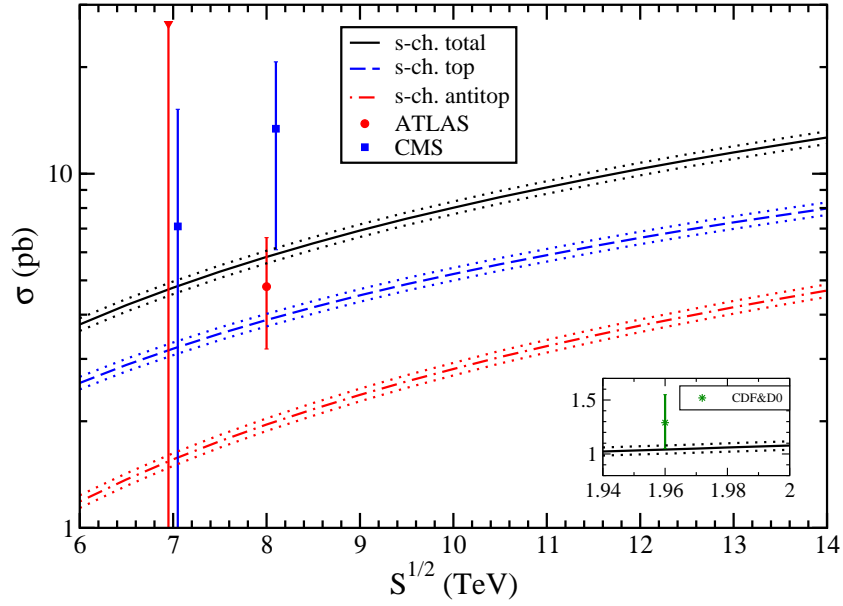


Figure 24: Single-top aNNLO production cross sections in the s -channel compared to ATLAS and CMS data at 7 TeV [141,142] and 8 TeV [142,143], and (inset) to CDF and D0 combination data [144] at 1.96 TeV.

$tW^- + \bar{t}W^+$ aN³LO cross section $m_t=172.5$ GeV

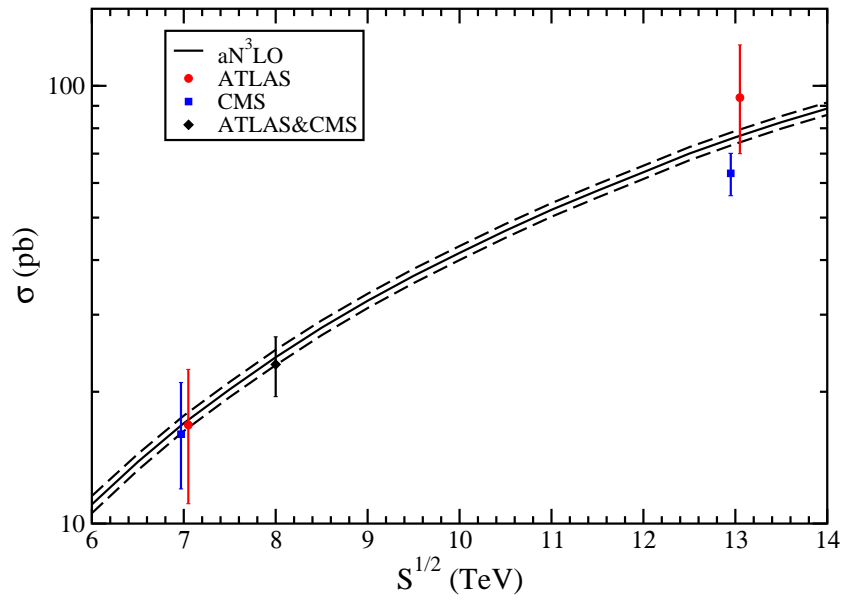


Figure 25: Single-top aN³LO production cross sections for tW production compared to ATLAS and CMS data at 7 TeV [145,146], 8 TeV [147], and 13 TeV [148,149].

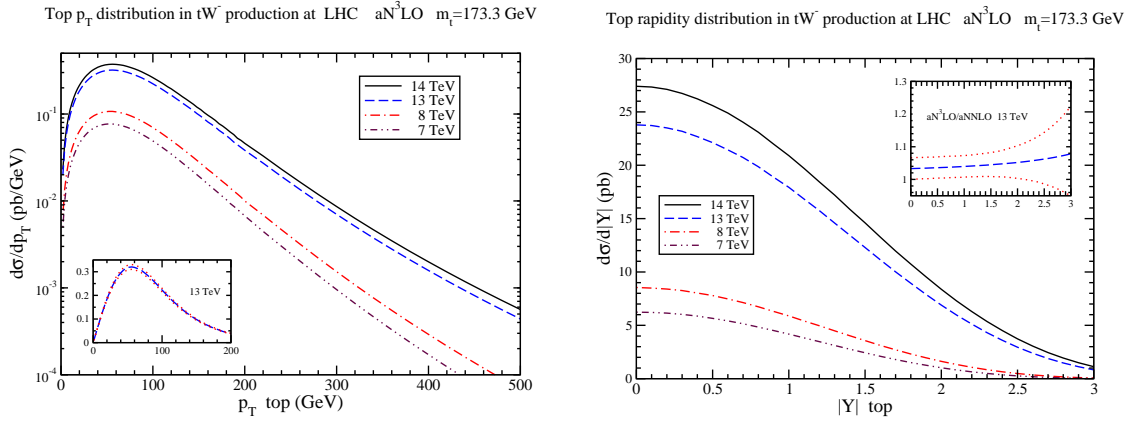


Figure 26: Top-quark p_T (left) and rapidity (right) aN^3LO distributions in tW^- production.



Figure 27: Lowest-order diagrams for the associated production of a top quark with a charged Higgs boson.

7 TeV, an ATLAS/CMS combination at 8 TeV [147], and ATLAS [148] and CMS [149] at 13 TeV.

Figure 26 displays the aN^3LO [77] top-quark p_T and rapidity distributions in tW^- production at LHC energies.

6 Top-quark production in models of new physics

In addition to the various Standard-Model processes for top-quark production, some of which we studied above, other possibilities include top production in association with particles in models of new physics, or top production via top-quark anomalous couplings. We consider some of these possibilities below.

6.1 Associated production of a top quark with a charged Higgs boson

We first consider the production of a top quark in association with a charged Higgs boson [71, 80, 83]. Charged Higgs bosons appear in the Minimal Supersymmetric Standard Model (MSSM) and other two-Higgs doublet models. The lowest-order diagrams for this process are shown in Fig. 27. The soft anomalous dimension for this process is the same as for tW production.

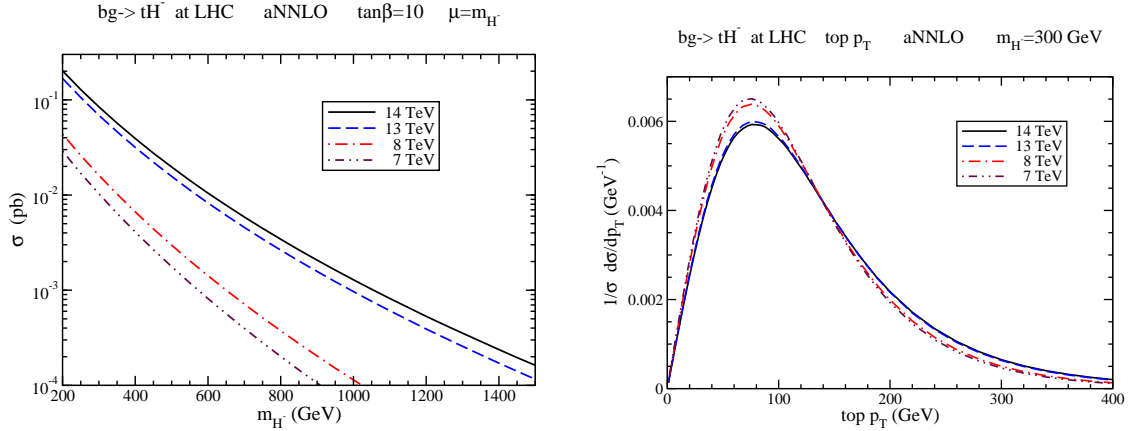


Figure 28: Total cross sections (left) and normalized top-quark p_T distributions (right) at aNNLO for charged-Higgs production in association with a top quark.

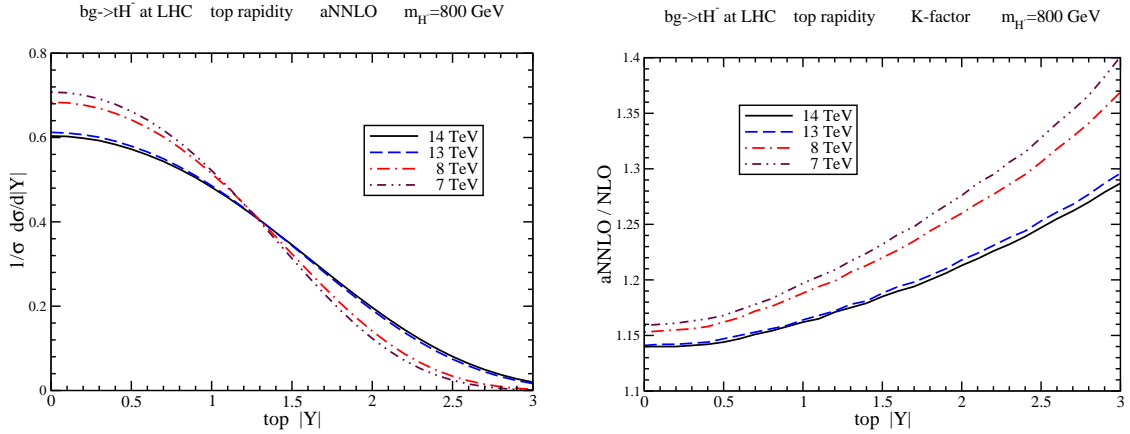


Figure 29: Normalized aNNLO top-quark rapidity distributions (left) and the corresponding K -factors (right) for charged-Higgs production in association with a top quark.

The left plot in Fig. 28 shows the aNNLO cross section for tH^- production in the MSSM, with $\tan\beta = 10$, at LHC energies as a function of charged-Higgs mass. The aNNLO corrections increase the NLO cross section significantly, with the particular value of the increase depending on the charged-Higgs mass. The plot on the right in Fig. 28 shows the aNNLO normalized top-quark p_T distributions in tH^- production for a charged-Higgs mass of 300 GeV.

The left plot of Fig. 29 shows the aNNLO top-quark rapidity distributions in tH^- production for a charged-Higgs mass of 800 GeV at LHC energies. The plot on the right in Fig. 29 shows the corresponding K factors, which are very considerable, especially at large rapidity.

6.2 Associated production of a top quark with a Z boson via anomalous couplings

An interesting process that involves top-quark anomalous couplings is the associated production of a top quark with a Z boson. While tZ production can proceed via Standard Model processes

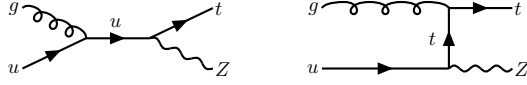


Figure 30: Lowest-order diagrams for the associated production of a top quark with a Z boson via anomalous t - q - Z coupling.

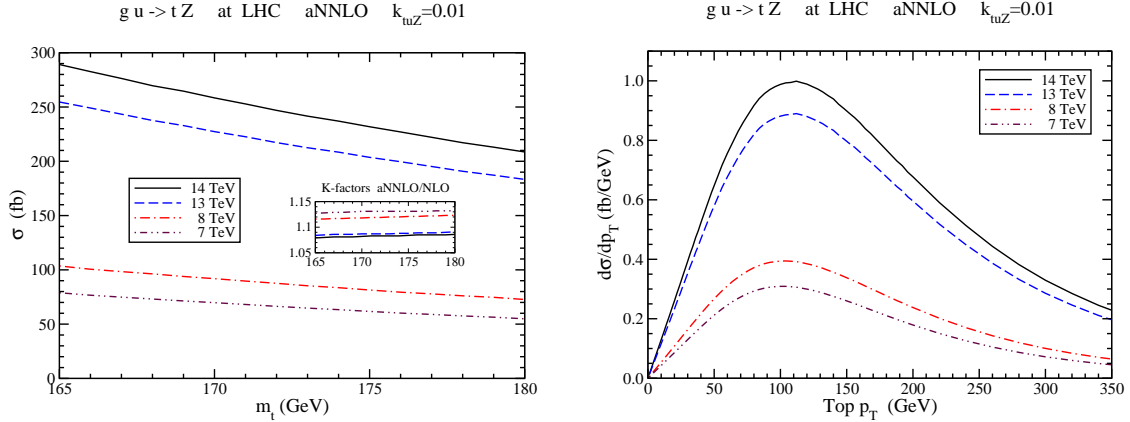


Figure 31: Total cross sections (left) and top-quark p_T distributions (right) at aNNLO for tZ production via anomalous couplings.

involving an additional quark in the final state, it is possible to produce a tZ final state without any other particles in models with anomalous couplings [79, 84]. The lowest-order diagrams are shown in Fig. 30.

An effective Lagrangian that includes an anomalous coupling of a t, q pair to a Z boson is

$$\Delta\mathcal{L}^{eff} = \frac{1}{\Lambda} \kappa_{tqZ} e \bar{t} \sigma_{\mu\nu} q F_Z^{\mu\nu} + h.c., \quad (48)$$

where κ_{tqZ} is the anomalous t - q - Z coupling with q an up or charm quark, $F_Z^{\mu\nu}$ is the Z -boson field tensor, $\sigma_{\mu\nu} = (i/2)(\gamma_\mu\gamma_\nu - \gamma_\nu\gamma_\mu)$ with Dirac matrices γ_μ , and Λ is an effective scale which we take to be the top-quark mass.

Soft-gluon corrections have been calculated at aNNLO in Ref. [84]. These soft corrections are important, and in fact at NLO they approximate the exact NLO [150] results remarkably well for both $gu \rightarrow tZ$ and $gc \rightarrow tZ$. The aNNLO corrections provide additional enhancements.

The left plot of Fig. 31 shows the aNNLO total cross sections for $gu \rightarrow tZ$ with $\kappa_{tuZ} = 0.01$ at 7, 8, 13, and 14 TeV LHC energies as functions of the top-quark mass, with scales set equal to the top-quark mass. The inset plot shows the aNNLO/NLO K -factors at the various LHC energies. The aNNLO corrections increase the NLO result significantly at all LHC energies.

The right plot of Fig. 31 shows the aNNLO top-quark p_T distributions, $d\sigma/dp_T$, at 7, 8, 13, and 14 TeV LHC energies with $m_t = 173.3$ GeV and $\kappa_{tuZ} = 0.01$.

6.3 Other top-quark production processes via anomalous couplings

In addition to tZ production discussed in the previous subsection, top quarks can also be produced in association with Z' or W' bosons [151] (see Ref. [152] for models of such particles). Soft-gluon corrections are significant for such processes [151].

The production of top quarks with photons, $gq \rightarrow t\gamma$, via anomalous $t-q-\gamma$ couplings, with q an up or charm quark, at Tevatron energy was studied in Ref. [79]. The soft-gluon corrections were found to be significant. The corrections are also large at LHC energies [153].

The process $eu \rightarrow et$ in electron-proton collisions via anomalous $t-u-\gamma$ coupling was studied in Ref. [78]. The processes $eq \rightarrow et$, with q an up or charm quark, via anomalous $t-q-\gamma$ and $t-q-Z$ couplings, were studied in Ref. [79]. The soft-gluon corrections were found to be important.

Same-sign top-quark production, $qq \rightarrow tt$, with q an up or charm quark, via anomalous $t-q-\gamma$ and $t-q-Z$ couplings, was studied in Ref. [79]. Numerical results were given for Tevatron energy [79].

The process $gu \rightarrow tg$ via anomalous $t-u-g$ couplings was studied in detail in Ref. [81]. The soft-gluon corrections were found to be substantial at LHC energies.

7 Summary

In this review, I have discussed soft-gluon corrections for top-quark production in hadronic collisions. I have presented the resummation of soft-gluon contributions in various top-quark processes through NNLL accuracy via two-loop calculations of soft anomalous dimension matrices.

N³LO approximate results with soft-gluon corrections for the $t\bar{t}$ production cross section, and the top-quark differential distributions in transverse momentum and rapidity, are in excellent agreement with data from the LHC and the Tevatron. Single-top cross sections and differential distributions have been presented in the t -channel and s -channel, and in tW production, and they are also in excellent agreement with collider data.

Top-quark production in association with charged-Higgs bosons or with anomalous couplings in models of new physics has also been discussed. Soft-gluon corrections are very significant for all top-quark production processes, and they reduce the theoretical errors.

Acknowledgments

This material is based upon work supported by the National Science Foundation under Grant No. PHY 1519606.

References

- [1] CDF Collab., *Phys. Rev. Lett.* **74**, 2626 (1995) [hep-ex/9503002].
- [2] D0 Collab., *Phys. Rev. Lett.* **74**, 2632 (1995) [hep-ex/9503003].

- [3] D0 Collab., *Phys. Rev. Lett.* **103**, 092001 (2009) [arXiv:0903.0850 [hep-ex]].
- [4] CDF Collab., *Phys. Rev. Lett.* **103**, 092002 (2009) [arXiv:0903.0885 [hep-ex]].
- [5] CMS Collab., *Phys. Lett. B* **695**, 424 (2011) [arXiv:1010.5994 [hep-ex]].
- [6] ATLAS Collab., *Eur. Phys. J. C* **71**, 1577 (2011) [arXiv:1012.1792 [hep-ex]].
- [7] E. Laenen, J. Smith and W.L. van Neerven, *Nucl. Phys. B* **369**, 543 (1992).
- [8] E. Laenen, J. Smith and W.L. van Neerven, *Phys. Lett. B* **321**, 254 (1994) [hep-ph/9310233].
- [9] N. Kidonakis and J. Smith, *Phys. Rev. D* **51**, 6092 (1995) [hep-ph/9502341].
- [10] E.L. Berger and H. Contopanagos, *Phys. Lett. B* **361**, 115 (1995) [hep-ph/9507363].
- [11] S. Catani, M.L. Mangano, P. Nason and L. Trentadue, *Phys. Lett. B* **378**, 329 (1996) [hep-ph/9602208].
- [12] E.L. Berger and H. Contopanagos, *Phys. Rev. D* **54**, 3085 (1996) [hep-ph/9603326].
- [13] N. Kidonakis and G. Sterman, *Phys. Lett. B* **387**, 867 (1996).
- [14] H. Contopanagos, E. Laenen and G. Sterman, *Nucl. Phys. B* **484**, 303 (1997) [hep-ph/9604313].
- [15] S. Catani, M.L. Mangano, P. Nason and L. Trentadue, *Nucl. Phys. B* **478**, 273 (1996) [hep-ph/9604351].
- [16] N. Kidonakis, J. Smith and R. Vogt, *Phys. Rev. D* **56**, 1553 (1997)[hep-ph/9608343].
- [17] N. Kidonakis and G. Sterman, *Nucl. Phys. B* **505**, 321 (1997) [hep-ph/9705234].
- [18] E.L. Berger and H. Contopanagos, *Phys. Rev. D* **57**, 253 (1998) [hep-ph/9706206].
- [19] R. Bonciani, S. Catani, M.L. Mangano and P. Nason, *Nucl. Phys. B* **529**, 424 (1998) [hep-ph/9801375].
- [20] E. Laenen, G. Oderda and G. Sterman, *Phys. Lett. B* **438**, 173 (1998) [hep-ph/9806467].
- [21] N. Kidonakis and R. Vogt, *Phys. Rev. D* **59**, 074014 (1999)[hep-ph/9806526].
- [22] N. Kidonakis, *Int. J. Mod. Phys. A* **15**, 1245 (2000) [hep-ph/9902484].
- [23] N. Kidonakis, *Phys. Rev. D* **64**, 014009 (2001) [hep-ph/0010002].
- [24] N. Kidonakis, E. Laenen, S. Moch and R. Vogt, *Phys. Rev. D* **64**, 114001 (2001) [hep-ph/0105041].
- [25] N. Kidonakis, *Int. J. Mod. Phys. A* **19**, 1793 (2004) [hep-ph/0303186].

- [26] R. Bonciani, S. Catani, M.L. Mangano and P. Nason, *Phys. Lett. B* **575**, 268 (2003) [hep-ph/0307035].
- [27] N. Kidonakis and R. Vogt, *Phys. Rev. D* **68**, 114014 (2003) [hep-ph/0308222].
- [28] N. Kidonakis, *Mod. Phys. Lett. A* **19**, 405 (2004) [hep-ph/0401147].
- [29] A. Banfi and E. Laenen, *Phys. Rev. D* **71**, 034003 (2005) [hep-ph/0411241].
- [30] N. Kidonakis, *Phys. Rev. D* **73**, 034001 (2006) [hep-ph/0509079].
- [31] S. Moch and P. Uwer, *Phys. Rev. D* **78**, 034003 (2008) [arXiv:0804.1476 [hep-ph]].
- [32] L.G. Almeida, G. Sterman and W. Vogelsang, *Phys. Rev. D* **78**, 014008 (2008) [arXiv:0805.1885 [hep-ph]].
- [33] N. Kidonakis and R. Vogt, *Phys. Rev. D* **78**, 074005 (2008) [arXiv:0805.3844 [hep-ph]].
- [34] Y. Kiyo, J.H. Kuhn, S. Moch, M. Steinhauser and P. Uwer, *Eur. Phys. J. C* **60**, 375 (2009) [arXiv:0812.0919 [hep-ph]].
- [35] N. Kidonakis, *Phys. Rev. Lett.* **102**, 232003 (2009) [arXiv:0903.2561 [hep-ph]].
- [36] A. Mitov, G. Sterman and I. Sung, *Phys. Rev. D* **79**, 094015 (2009) [arXiv:0903.3241 [hep-ph]].
- [37] T. Becher and M. Neubert, *Phys. Rev. D* **79**, 125004 (2009) [Erratum: *ibid.* **80**, 109901 (2009)] [arXiv:0904.1021 [hep-ph]].
- [38] M. Beneke, P. Falgari and C. Schwinn, *Nucl. Phys. B* **828**, 69 (2010) [arXiv:0907.1443 [hep-ph]].
- [39] M. Czakon, A. Mitov and G. Sterman, *Phys. Rev. D* **80**, 074017 (2009) [arXiv:0907.1790 [hep-ph]].
- [40] A. Ferroglia, M. Neubert, B.D. Pecjak and L.L. Yang, *Phys. Rev. Lett.* **103**, 201601 (2009) [arXiv:0907.4791 [hep-ph]].
- [41] A. Ferroglia, M. Neubert, B.D. Pecjak and L.L. Yang, *JHEP* **0911**, 062 (2009) [arXiv:0908.3676 [hep-ph]].
- [42] I. Sung, *Phys. Rev. D* **80**, 094020 (2009) [arXiv:0908.3688 [hep-ph]].
- [43] M. Beneke, M. Czakon, P. Falgari, A. Mitov and C. Schwinn *Phys. Lett. B* **690**, 483 (2010) [arXiv:0911.5166 [hep-ph]].
- [44] V. Ahrens, A. Ferroglia, M. Neubert, B.D. Pecjak and L.L. Yang, *Phys. Lett. B* **687**, 331 (2010) [arXiv:0912.3375 [hep-ph]].
- [45] V. Ahrens, A. Ferroglia, M. Neubert, B.D. Pecjak and L.L. Yang, *JHEP* **1009**, 097 (2010) [arXiv:1003.5827 [hep-ph]].

- [46] A. Mitov, G. Sterman and I. Sung, *Phys. Rev. D* **82**, 034020 (2010) [arXiv:1005.4646 [hep-ph]].
- [47] M. Aliev, H. Lacker, U. Langenfeld, S. Moch, P. Uwer and M. Wiedemann, *Comput. Phys. Commun.* **182**, 1034 (2011) [arXiv:1007.1327 [hep-ph]].
- [48] M. Beneke, P. Falgari and C. Schwinn, *Nucl. Phys. B* **842**, 414 (2011) [arXiv:1007.5414 [hep-ph]].
- [49] N. Kidonakis, *Phys. Rev. D* **82**, 114030 (2010) [arXiv:1009.4935 [hep-ph]].
- [50] V. Ahrens, A. Ferroglia, M. Neubert, B.D. Pecjak and L.L. Yang, *JHEP* **1109**, 070 (2011) [arXiv:1103.0550 [hep-ph]].
- [51] N. Kidonakis, *Phys. Rev. D* **84**, 011504(R) (2011) [arXiv:1105.5167 [hep-ph]].
- [52] V. Ahrens, A. Ferroglia, M. Neubert, B.D. Pecjak and L.L. Yang, *Phys. Lett. B* **703**, 135 (2011) [arXiv:1105.5824 [hep-ph]].
- [53] N. Kidonakis and B.D. Pecjak, *Eur. Phys. J. C* **72**, 2084 (2012) [arXiv:1108.6063 [hep-ph]].
- [54] M. Beneke, P. Falgari, S. Klein and C. Schwinn, *Nucl. Phys. B* **855**, 695 (2012) [arXiv:1109.1536 [hep-ph]].
- [55] M. Cacciari, M. Czakon, M. Mangano, A. Mitov and P. Nason, *Phys. Lett. B* **710**, 612 (2012) [arXiv:1111.5869 [hep-ph]].
- [56] S. Moch, P. Uwer and A. Vogt, *Phys. Lett. B* **714**, 48 (2012) [arXiv:1203.6282 [hep-ph]].
- [57] A. Ferroglia, B.D. Pecjak and L.L. Yang, *Phys. Rev. D* **86**, 034010 (2012) [arXiv:1205.3662 [hep-ph]].
- [58] M. Beneke, P. Falgari, S. Klein, J. Piclum, C. Schwinn, M. Ubiali and F. Yan, *JHEP* **1207**, 194 (2012) [arXiv:1206.2454 [hep-ph]].
- [59] N. Kidonakis, *Phys. Part. Nucl.* **45**, 714 (2014) [arXiv:1210.7813 [hep-ph]].
- [60] N. Kidonakis, in *Proceedings of the Helmholtz International School Physics of Heavy Quarks and Hadrons, HQ2013*, Dubna, Russia, 2013, DESY-PROC-2013-03, p. 139 [arXiv:1311.0283 [hep-ph]].
- [61] N. Kidonakis, *Phys. Rev. D* **90**, 014006 (2014) [arXiv:1405.7046 [hep-ph]].
- [62] M. Guzzi, K. Lipka and S.-O. Moch, *JHEP* **1501**, 082 (2015) [arXiv:1406.0386 [hep-ph]].
- [63] A. Broggio, A.S. Papanastasiou and A. Signer, *JHEP* **1410**, 98 (2014) [arXiv:1407.2532 [hep-ph]].
- [64] N. Kidonakis, *Phys. Rev. D* **91**, 031501(R) (2015) [arXiv:1411.2633 [hep-ph]].

- [65] N. Kidonakis, *Phys. Rev. D* **91**, 071502(R) (2015) [arXiv:1501.01581 [hep-ph]].
- [66] C. Muselli, M. Bonvini, S. Forte, S. Marzani and G. Ridolfi, *JHEP* **1508**, 076 (2015) [arXiv:1505.02006 [hep-ph]].
- [67] G. Wang, X. Xu, L.L. Yang and H.X. Zhu, arXiv:1804.05218 [hep-ph].
- [68] N. Kidonakis, *Phys. Rev. D* **74**, 114012 (2006) [hep-ph/0609287].
- [69] N. Kidonakis, *Phys. Rev. D* **75**, 071501(R) (2007) [hep-ph/0701080].
- [70] N. Kidonakis, *Phys. Rev. D* **81**, 054028 (2010) [arXiv:1001.5034 [hep-ph]].
- [71] N. Kidonakis, *Phys. Rev. D* **82**, 054018 (2010) [arXiv:1005.4451 [hep-ph]].
- [72] H.X. Zhu, C.S. Li, J. Wang and J.J. Zhang, *JHEP* **1102**, 099 (2011) [arXiv:1006.0681 [hep-ph]].
- [73] N. Kidonakis, *Phys. Rev. D* **83**, 091503(R) (2011) [arXiv:1103.2792 [hep-ph]].
- [74] J. Wang, C.S. Li and H.X. Zhu, *Phys. Rev. D* **87**, 034030 (2013) [arXiv:1210.7698 [hep-ph]].
- [75] N. Kidonakis, *Phys. Rev. D* **88**, 031504(R) (2013) [arXiv:1306.3592 [hep-ph]].
- [76] N. Kidonakis, *Phys. Rev. D* **93**, 054022 (2016) [arXiv:1510.06361 [hep-ph]].
- [77] N. Kidonakis, *Phys. Rev. D* **96**, 034014 (2017) [arXiv:1612.06426 [hep-ph]].
- [78] A. Belyaev and N. Kidonakis, *Phys. Rev. D* **65**, 037501 (2002) [hep-ph/0102072].
- [79] N. Kidonakis and A. Belyaev, *JHEP* **0312**, 004 (2003) [hep-ph/0310299].
- [80] N. Kidonakis, *JHEP* **0505**, 011 (2005) [hep-ph/0412422].
- [81] N. Kidonakis and E. Martin, *Phys. Rev. D* **90**, 054021 (2014) [arXiv:1404.7488 [hep-ph]].
- [82] L.L. Yang, C.S. Li, J. Gao and J. Wang, *JHEP* **1412**, 123 (2014) [arXiv:1409.6959 [hep-ph]].
- [83] N. Kidonakis, *Phys. Rev. D* **94**, 014010 (2016) [arXiv:1605.00622 [hep-ph]].
- [84] N. Kidonakis, *Phys. Rev. D* **97**, 034028 (2018) [arXiv:1712.01144 [hep-ph]].
- [85] P. Nason, S. Dawson and R.K. Ellis, *Nucl. Phys. B* **303**, 607 (1988).
- [86] W. Beenakker, H. Kuijf, W.L. van Neerven and J. Smith, *Phys. Rev. D* **40**, 54 (1989).
- [87] W. Beenakker, W.L. van Neerven, R. Meng, G.A. Schuler and J. Smith, *Nucl. Phys. B* **351**, 507 (1991).

- [88] M. Czakon, P. Fiedler and A. Mitov, *Phys. Rev. Lett.* **110**, 252004 (2013) [arXiv:1303.6254 [hep-ph]].
- [89] M. Czakon, P. Fiedler and A. Mitov, *Phys. Rev. Lett.* **115**, 052001 (2015) [arXiv:1411.3007 [hep-ph]].
- [90] M. Czakon, D. Heymes and A. Mitov, *Phys. Rev. Lett.* **116**, 082003 (2016) [arXiv:1511.00549 [hep-ph]].
- [91] M. Czakon, P. Fiedler, D. Heymes and A. Mitov, *JHEP* **1605**, 034 (2016) [arXiv:1601.05375 [hep-ph]].
- [92] B.W. Harris, E. Laenen, L. Phaf, Z. Sullivan and S. Weinzierl, *Phys. Rev. D* **66**, 054024 (2002) [hep-ph/0207055].
- [93] S.H. Zhu, *Phys. Lett. B* **524**, 283 (2002) [Erratum: *ibid.* **537**, 351 (2002)] [hep-ph/0109269].
- [94] M. Brucherseifer, F. Caola and K. Melnikov, *Phys. Lett. B* **736**, 58 (2014) [arXiv:1404.7116 [hep-ph]].
- [95] E.L. Berger, J. Gao, C.-P. Yuan, and H.X. Zhu, *Phys. Rev. D* **94**, 071501 (2016) [arXiv:1606.08463 [hep-ph]].
- [96] E.L. Berger, J. Gao, and H.X. Zhu, *JHEP* **1711**, 158 (2017) [arXiv:1708.09405 [hep-ph]].
- [97] G. Sterman, *Nucl. Phys. B* **281**, 310 (1987).
- [98] S. Catani and L. Trentadue, *Nucl. Phys. B* **327**, 323 (1989).
- [99] J. Kodaira and L. Trentadue, *Phys. Lett.* **112B**, 66 (1982).
- [100] G.P. Korchemsky and A.V. Radyushkin, *Nucl. Phys. B* **283**, 342 (1987).
- [101] A. Grozin, J.M. Henn, G.P. Korchemsky and P. Marquard, *Phys. Rev. Lett.* **114**, 062006 (2015) [arXiv:1409.0023 [hep-ph]].
- [102] N. Kidonakis, *Int. J. Mod. Phys. A* **31**, 1650076 (2016) [arXiv:1601.01666 [hep-ph]].
- [103] A.D. Martin, W.J. Stirling, R.S. Thorne and G. Watt, *Eur. Phys. J. C* **63**, 189 (2009) [arXiv:0901.0002 [hep-ph]].
- [104] L.A. Harland-Lang, A.D. Martin, P. Molytinski and R.S. Thorne, *Eur. Phys. J. C* **75**, 204 (2015) [arXiv:1412.3989 [hep-ph]].
- [105] S. Dulat, T.-J. Hou, J. Gao, M. Guzzi, J. Huston, P. Nadolsky, J. Pumplin, C. Schmidt, D. Stump and C.-P. Yuan, *Phys. Rev. D* **93**, 033006 (2016) [arXiv:1506.07443 [hep-ph]].
- [106] NNPDF Collaboration, R.D. Ball *et al.*, *Eur. Phys. J. C* **77**, 663 (2017) [arXiv:1706.00428 [hep-ph]].

- [107] CMS Collab., *JHEP* **1803**, 115 (2018) [arXiv:1711.03143 [hep-ex]].
- [108] ATLAS Collab., *Eur. Phys. J. C* **74**, 3109 (2014) [Addendum: *ibid.* **76**, 642 (2016)] [arXiv:1406.5375 [hep-ex]].
- [109] CMS Collab., *JHEP* **1608**, 029 (2016) [arXiv:1603.02303 [hep-ex]].
- [110] ATLAS Collab., arXiv:1712.06857 [hep-ex].
- [111] ATLAS Collab., *Phys. Lett. B* **761**, 136 (2016) [Erratum: *ibid.* **772**, 879 (2017)] [arXiv:1606.02699 [hep-ex]].
- [112] CMS Collab., *JHEP* **1709**, 051 (2017) [arXiv:1701.06228 [hep-ex]].
- [113] CDF Collab., *Phys. Rev. D* **64**, 032002 (2001) [Erratum: *ibid.* **67**, 119901 (2003)] [hep-ex/0101036].
- [114] D0 Collab., *Phys. Rev. D* **67**, 012004 (2003) [hep-ex/0205019].
- [115] CDF and D0 Collab., *Phys. Rev. D* **89**, 072001 (2014) [arXiv:1309.7570 [hep-ex]].
- [116] CMS Collab., *JHEP* **1804**, 060 (2018) [arXiv:1708.07638 [hep-ex]].
- [117] ATLAS Collab., *Eur. Phys. J. C* **76**, 538 (2016) [arXiv:1511.04716 [hep-ex]].
- [118] CMS Collab., *Eur. Phys. J. C* **75**, 542 (2015) [arXiv:1505.04480 [hep-ex]].
- [119] ATLAS Collab., *Phys. Rev. D* **93**, 032009 (2016) [arXiv:1510.03818 [hep-ex]].
- [120] CMS Collab., *Phys. Rev. D* **94**, 072002 (2016) [arXiv:1605.00116 [hep-ex]].
- [121] CMS Collab., *Eur. Phys. J. C* **73**, 2339 (2013) [arXiv:1211.2220 [hep-ex]].
- [122] ATLAS Collab., *Phys. Rev. D* **90**, 072004 (2014) [arXiv:1407.0371 [hep-ex]].
- [123] D0 Collab., *Phys. Rev. D* **90**, 092006 (2014) [arXiv:1401.5785 [hep-ex]].
- [124] W. Bernreuther and Z.-G. Si, *Phys. Rev. D* **86**, 034026 (2012) [arXiv:1205.6580 [hep-ph]].
- [125] W. Bernreuther and Z.-G. Si, *Nucl. Phys. B* **837**, 90 (2010) [arXiv:1003.3926 [hep-ph]].
- [126] W. Hollik and D. Pagani, *Phys. Rev. D* **84**, 093003 (2011) [arXiv:1107.2606 [hep-ph]].
- [127] A.V. Manohar and M. Trott, *Phys. Lett. B* **711**, 313 (2012) [arXiv:1201.3926 [hep-ph]].
- [128] D. Pagani, I. Tsinikos and M. Zaro, *Eur. Phys. J. C* **76**, 479 (2016) [arXiv:1606.01915 [hep-ph]].
- [129] CDF and D0 Collab., *Phys. Rev. Lett.* **120**, 042001 [arXiv:1709.04894 [hep-ex]].
- [130] D0 Collab., *Phys. Rev. D* **90**, 072011 (2014) [arXiv:1405.0421 [hep-ex]].

- [131] CDF Collab., *Phys. Rev. D* **93**, 112005 (2016) [arXiv:1602.09015 [hep-ex]].
- [132] CDF and D0 Collab., *Phys. Rev. Lett.* **115**, 152003 (2015) [arXiv:1503.05027 [hep-ex]].
- [133] CMS Collab., *JHEP* **1212**, 035 (2012) [arXiv:1209.4533 [hep-ex]].
- [134] ATLAS Collab., *Phys. Rev. D* **90**, 112006 (2014) [arXiv:1406.7844 [hep-ex]].
- [135] CMS Collab., *JHEP* **1406**, 090 (2014) [arXiv:1403.7366 [hep-ex]].
- [136] ATLAS Collab., *Eur. Phys. J. C* **77**, 531 (2017) [arXiv:1702.02859 [hep-ex]].
- [137] ATLAS Collab., *JHEP* **1704**, 086 (2017) [arXiv:1609.03920 [hep-ex]].
- [138] CMS Collab., *Phys. Lett. B* **772**, 752 (2017) [arXiv:1610.00678 [hep-ex]].
- [139] CMS Collab., CMS-PAS-TOP-14-004.
- [140] CMS Collab., CMS-PAS-TOP-16-004.
- [141] ATLAS Collab., ATLAS-CONF-2011-118.
- [142] CMS Collab., *JHEP* **1609**, 027 (2016) [arXiv:1603.02555 [hep-ex]].
- [143] ATLAS Collab., *Phys. Lett. B* **756**, 228 (2016) [arXiv:1511.05980 [hep-ex]].
- [144] CDF and D0 Collab., *Phys. Rev. Lett.* **112**, 231803 (2014) [arXiv:1402.5126 [hep-ex]].
- [145] ATLAS Collab., *Phys. Lett. B* **716**, 142 (2012) [arXiv:1205.5764 [hep-ex]].
- [146] CMS Collab., *Phys. Rev. Lett.* **110**, 022003 (2013) [arXiv:1209.3489 [hep-ex]].
- [147] ATLAS and CMS Collab., ATLAS-CONF-2016-023, CMS-PAS-TOP-15-019.
- [148] ATLAS Collab., *JHEP* **1801**, 063 (2018) [arXiv:1612.07231 [hep-ex]].
- [149] CMS Collab., arXiv:1805.07399 [hep-ex].
- [150] B.H. Li, Y. Zhang, C.S. Li, J. Gao, and H.X. Zhu, *Phys. Rev. D* **83**, 114049 (2011) [arXiv:1103.5122 [hep-ph]].
- [151] M. Guzzi and N. Kidonakis, in preparation.
- [152] A. Faraggi and M. Guzzi, *Eur. Phys. J. C* **75**, 537 (2015) [arXiv:1507.07406 [hep-ph]].
- [153] M. Forsslund and N. Kidonakis, in preparation.